N73-16534

NASA CR-121131
PWA^{TM}-4593

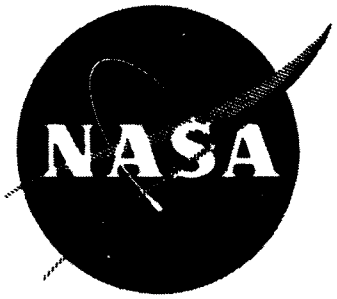

LABYRINTH SEAL TESTING FOR LIFT FAN ENGINES

by
L. J. Dobek

PRATT & WHITNEY AIRCRAFT
DIVISION OF UNITED AIRCRAFT CORPORATION

Prepared For

NATIONAL AERONAUTICS AND SPACE ADMINISTRATION

NASA LEWIS RESEARCH CENTER
CONTRACT NAS3-14409

1. Report No.	2. Government Accession No.	3. Recipient's Catalog No.
NASA CR-121131		

4. Title and Subtitle	5. Report Date
Labyrinth Seal Testing For Lift Fan Engines	February 1973
	6. Performing Organization Code
7. Author(s)	8. Performing Organization Report No.
L. J. Dobek	PWA^{TM}-4593
	10. Work Unit No.
9. Performing Organization Name and Address	
Pratt & Whitney Aircraft Division of United Aircraft Corporation East Hartford, Connecticut 06108	11. Contract or Grant No. NAS 3-14409
	13. Type of Report and Period Covered
12. Sponsoring Agency Name and Address	Contractor Report
National Aeronautics and Space Administration Washington, D. C. 20546	14. Sponsoring Agency Code

15. Supplementary Notes

Project Manager, Thomas N. Strom, Power Procurement Section, NASA Lewis Research Center, Cleveland, Ohio

16. Abstract

An abradable buffered labyrinth seal for the control of turbine gas path leakage in a tip-turbine driven lift fan was designed, tested, and analyzed. The seal configuration was not designed to operate in any specific location but was sized to be evaluated in an existing test rig. The final sealing diameter selected was 71.12 x 10^{-2} meters (28 inches). Results of testing indicate that the flow equations predicted seal air flows consistent with measured values. Excellent sealing characteristics of the abradable coating on the stator land were demonstrated when a substantial seal penetration of .076 x 10^{-2} meter (.030 inch) into the land surface was enountered without appreciable wear on the labyrinth knife edges.

17. Key Words (Suggested by Author(s))	18. Distribution Statement
Labyrinth Seal Lift Fan Tip Turbine Seals Buffered Seals	

19. Security Classif. (of this report)	20. Security Classif. (of this page)	21. No. of Pages	22. Price*
Unclassified	Unclassified	78	

* For sale by the National Technical Information Service, Springfield, Virginia 22151

FOREWORD

This report describes the work accomplished on contract NAS3-14409 by the Pratt & Whitney Aircraft Division of United Aircraft Corporation for the Lewis Research Center of the National Aeronautics & Space Adminstration. The work was initiated 18 February 1971 and completed on 17 October 1972.

Thomas N. Strom of the National Aeronautics & Space Administration Fluid Systems Components Division was Project Manager and Leonard W. Schopen, NASA Lewis Research Center was the Contracting Officer.

Oscar Stewart was Program Manager for Pratt & Whitney Aircraft from the inception of this contract until 31 December 1971. From 1 January 1972 until 31 August 1972, Valentine P. Povinelli was Program Manager and from 1 Sept. 1972 until contract completion Louis J. Dobek was the Program Manager.

An expression of appreciation is extended to Wellington J. Walker and Philip R. Lawell for assistance in the preparation of material for this report.

Table of Contents

LIST OF FIGURES

LIST OF FIGURES (Cont'd)

LIST OF FIGURES

LABYRINTH SEAL TESTING FOR LIFT FAN ENGINES

L. J. Dobek
Pratt & Whitney Aircraft Division
United Aircraft Corporation

I SUMMARY

This report presents the work accomplished under Contract NAS3-14409 from its initiation on 18 February 1971 to completion of the technical program on 17 October 1972. The specific objective of this program was to flow calibrate a buffered labyrinth seal under environmental conditions similar to those expected at the first-stage inner air seal of a lift fan tip turbine.

Task I was a design analysis program which developed an equation for a generalized solution of buffered labyrinth seals. The seal design which was selected for experimental evaluation in an existing test rig was a combined single and two stage labyrinth seal. In such a seal, buffer gas is introduced through radial orifices in the stationary seal land between the single stage labyrinth and the double stage labyrinth. Gas splits and flows axially across the labyrinth. The concept is to seal the high temperature tip turbine gas down stream of the single labyrinth from the ambient gas flow of the fan downstream of the two stage labyrinth. The seal consists of an AMS 5660 nickel alloy machined ring of continuous knife edges mounted on a rotor disk. The land is formed by the I.D. of the buffer gas manifold coated with METCO 601 plasma spray abradable material. The substrate material is AMS 5613 stainless steel.

From the analysis, two static cold knife edge clearances were selected that would provide operating clearances ranging from 1.27×10^{-3} meters (.050 inch) to less than $.254 \times 10^{-3}$ meters (.010 inch). The analysis considered thermal and structural response of the seal components.

Experimental evaluation of the seal was accomplished in two builds. In build I, a cold static seal clearance of approximately 1.27×10^{-3} meters (.050 inch) was used. The clearance in build 2 was set at $.302 \times 10^{-3}$ meter (.020 inch). A room temperature static unidirectional flow calibration was performed for each build. From the results, the buffer gas orifice flow coefficient was determined to be 0.8. The unidirectional gas flow across the double and single labyrinths compared favorably with analytical predictions.

The two directional flow calibration was made at a sealed gas pressure of approximately 172.4×10^3 N/m^2 (25 psia). Buffer gas pressure was varied from 200.7×10^3 N/m^2 (30 psia) to 262×10^3 N/m^2 (38 psia). The ambient gas compartment was evacuated to less than 124.1×10^3 N/m^2 (18 psia) for all test points. Buffer gas temperatures were set at 294°K (70°F), 394°K (250°F) and 461°K (370°F). Primary gas was heated as a result of mixing with buffer gas leakage except during test points at which 922°K (1200°F) air was delivered to the primary gas compartment. The calibration was performed at a combination of the above pressures and temperatures at rotor speeds from static to 5950 rpm.

Calibration results of the buffer orifice flows and its subsequential flow split across the single and double knife edge labyrinths showed good correlation with analytically determined values at static and dynamic conditions. Buffer orifice flows were measured to be within 10 percent of predicted values at the larger knife edge clearances and within 20 percent at the smaller clearances. The flow split across the labyrinth seals for any measured orifice flow was found to be in the range of 11 percent of the calculated value.

II INTRODUCTION

Advanced flight engines present continuing requirements for high operating speeds, large engine structures of minimum weight, and maximum operating efficiency. In combination, these requirements lead to large-diameter rotating air seals which must operate at high speed, and with minimum clearance, in a relatively flexible structure. Such seals, and particularly fan seals, have the potential for large radial excursions due to maneuver loads, engine surge, dynamic unbalance loads, and structural creep. In order to use minimum-clearance labyrinth seals under these conditions, it is desirable to incorporate an abradable material in the sealing land. Most of the wear resulting from a rub will then occur in the land, and only a local increase in seal leakage will be experienced.

The specific intent of NASA-Lewis Contract NAS 3-14409 was to design, analyze, fabricate, and rig test a buffered abradable labyrinth seal for a lift fan engine application. Selection of a "buffered" abradable type labyrinth seal was made over a "straight-thru" type because the buffered scheme eases the differential thermal response of the seal and structural components at transient conditions. Clearance control becomes simpler and there is a reduction in the risk of knife edge interaction with the land. Also, it can be expected that the hot turbine gas leakage to the fan air flow stream would be eliminated. The design was to be functionally similar to the first stage turbine seal concept for the two-stage turbine shown on National Aeronautics and Space Administration - Lewis Research Center drawing No. CR-6550807. It was not the intent of this contract to duplicate the structural and thermal response of any particular seal application. The seal was designed for testing in an existing test rig used previously under Contract NAS 3-7605 with its sealing diameter to be at least 71.12×10^{-2} meters (28 inches).

Basic seal design requirements included a relatively high operating temperature and a minimum clearance at high operating speeds while maintaining the lowest possible weight. These requirements imply a highly stressed rotating member in which creep and distortions due to thermal effects and pressure loads are important design considerations. The stationary part of the seal does not experience inertia loads but does operate at elevated temperatures, is exposed to pressure loading, is able to wear under rubbing conditions without inducing wear on the knife-edge, and does preferably experience dimensional changes in operation which correspond to those of the rotating member. In consequence, the labyrinth seal becomes a highly sophisticated component in the lift-fan engine application.

III. CONCLUSIONS AND RECOMMENDATIONS

The calibration of an abradable buffered labyrinth seal under this contract revealed the following:

- Results of the static unidirectional flow calibration of the buffered labyrinth design at two cold gap clearances demonstrated good correlation between measured and calculated air flows.

- Experimental calibration of the seal buffer gas orifices revealed the flow coefficient (0.8) to be higher than would be selected in conventional practice.

- Measured air flows through the double knife edge seal to the ambient compartment during dynamic testing were lower than the calculated values.

- Measured flows through the buffer orifices during dynamic seal testing showed good correlation with calculated values at the large "cold" knife edge gap. Reducing the knife edge clearance did not result in the same good correlation between measured and calculated buffer flows, reflecting the increased sensitivity of the discharge coefficient (α) with decreasing seal clearance.

- Measured knife edge clearances during dynamic testing were consistently tighter than predicted values due to the higher than anticipated rotor temperature and resultant rotor growth.

- The seal stator rub-strip of METCO 601 demonstrated excellent abradable characteristics with a deep knife edge penetration. No significant knife edge wear or distress resulted.

In consideration of the above observations the following conclusions can be made of this seal in the range of conditions studied:

- The flow equations developed were proven to be within 20 percent accuracy in calculating airflows across the seals.

- The flow coefficient for a particular buffer orifice configuration should be obtained experimentally.

- Acceptable analytical methods are available to calculate buffer air flow.

Based on test and analytical experience gained during this contract it is recommended by the Contractor that:

- For specific geometric configurations, the buffer orifice should be experimentally calibrated to insure accurate determination of the flow coefficient.

- In selecting the minimum cold seal gap, a thorough thermal and flow analysis of the specific seal design and surrounding structure is necessary to minimize the possibilities of a severe seal rub.

- Further experimental and analytical investigation is necessary to accurately select the Egli parameters used in calculating air flow through the double knife edge seals.

IV TECHNICAL PROGRAM

The technical program effort under NASA-Lewis Contract NAS-3-14409 consisted of three separate tasks. Task I included the design analysis of a buffered abradable labyrinth seal that could be evaluated in an existing test rig. Effort here also included the detail seal design and the detail design modification of a seal rig which would be used for evaluation of the seal. Task II entailed the procurement of the test seal and rig hardware. Experimental evaluation of the seal, and analysis of the test results were conducted in Task III.

A. SEAL DESIGN ANALYSIS

The seal design was documented for this contract, based upon analytical and design studies of a buffered abradable labyrinth seal for the control of turbine gas path leakage in a tip-turbine driven lift fan. The design analysis was performed on a seal similar in cross-section to an engine seal but reduced to a 71.12×10^{-2} meter (28 inch) diameter to operate in an existing test rig.

The specific steps performed in independently determining the seal characteristics are presented in the flow, thermal, and structural analysis sections. Integration of these three independent analyses is then presented in the seal performance analysis section.

1. Flow Analysis

Flow analysis of the buffered labyrinth seal consisted of examining three separate interconnected flow paths. Figure 1 is a schematic diagram of the flow system. W_1 is the flow of buffer air through orifices to an intermediate location between the knife edges (P_I, T_I). W_2 is the flow through the double knife edge to ambient air (P_A,T_A) and W_3 is the flow through the single knife edge to the primary region (P_P,T_P). The buffered labyrinth seal design concept further requires that the following pressure relationships apply to the flow system:

Case I	$P_B > P_I > P_P > P_A$	; $W_1 = W_2 + W_3$	(Eq.1)
Case II	$P_B > P_I = P_P > P_A$	; $W_1 = W_2$	(Eq.2)
Case III	$P_B > P_I < P_P > P_A$	; $W_1 = W_2 - W_3$	(Eq.3)

The relative magnitude of P_I depends on the flow areas in the system, and the three continuity equations defined as Cases I, II, and III are the only flow relationships which could apply. Cases II and III result in an unfavorable thermal situation, which will be examined in more detail in the thermal and structural sections of this report. Case I, in which W_3 flow exists and is always from the intermediate location to the primary region, is the only situation which can be allowed to exist. This restriction places a maximum allowable value on knife edge clearance.

Orifice flow (W_1) is defined by the equation (ref. 1):

$$W_1 = N_o \left[K_f A_o Y \sqrt{2g \rho_B (P_B - P_I)} \right] \quad \text{(Eq.4)}$$

N_o = number of orifices

Ao = orifice area

ρ_B = density of buffer air

P_B = pressure of buffer air

P_I = pressure of intermediate air

$$Y = \text{expansion factor} = \sqrt{\frac{k}{k-1}\left[\left(\frac{P_I}{P_B}\right)^{2/k} - \left(\frac{P_I}{P_B}\right)^{\frac{(k+1)}{k}}\right]} \Bigg/ \sqrt{\frac{P_B - P_I}{P_B}} \quad \text{(Eq.5) (Ref. 1)}$$

k = specific heat ratio

K_f = flow coefficient = .6 for square edged orifices

If geometry and buffer air conditions are chosen, W_1 becomes a function of P_I alone.

The Egli analysis (ref. 2), which is generally applied to multi-stage labyrinth seals, is particularly relevant when analyzing "straight through" seals in which flow carry-over between knife edges is significant.

$$W = A\phi\alpha\gamma\sqrt{g\rho_u P_u} \quad \text{(Eq.6)}$$

A = leakage area

ϕ = flow function = function of N, P_d/P_u

α = flow coefficient = function of t, e/t

γ = carry-over factor = function of N, e/s

P_u = upstream pressure

ρ_u = upstream density

N = number of knife edges

e = knife edge clearance

t = knife edge thickness

s = knife edge spacing

P_d = downstream pressure

The values of ϕ, α and γ are obtained from the graphs in Figure 2. The specific equations for W_2 and W_3 are:

$$W_2 = A\phi_2 \left(\alpha\gamma\sqrt{g\rho_I P_I}\right) \qquad \text{Where } P_d = P_A \; N = 2 \qquad \text{(Eq.7)}$$

$$W_3 = A\phi_3 \left(\alpha\sqrt{g\rho_I P_I}\right) \qquad \text{Where } P_d = P_P, \; N = 1 \qquad \text{(Eq.8)}$$

The carry-over factor is unity for a single knife edge. Values used for knife edge thickness and spacing are $.048 \times 10^{-2}$ meter (.019 inch) and $.409 \times 10^{-2}$ meter (.161 inch), respectively. Specifying the knife edge clearance (e), W_2 and W_3 may be expressed as functions of intermediate pressure P_I.

A design constraint exists in which the intermediate pressure cannot be less than the primary air pressure (the later pressure is dictated by performance requirements) since this condition would cause primary air flow across the seal (Case III). When the intermediate pressure is equal to the primary pressure (Case II), a maximum allowable clearance is established although in practice the seal would not be designed to operate to this limit

Using the Case I flow relationship, the continuity equation (eq.1) is used to obtain intermediate pressure for various values of seal clearance for any given size and number of buffer gas orifices and buffer gas pressures, P_B.

If: $W_1 = W_2 + W_3$

then: $N_o \left(K_f A_o Y \sqrt{2g\rho_B (P_B - P_I)}\right) = A\phi_2\alpha\gamma\sqrt{g\rho_I P_I}$

$$+ A\phi_3\alpha\sqrt{g\rho_I P_I} \qquad \text{(Eq. 9)}$$

For a buffer gas manifold with 152 orifices of 5.3×10^{-3} meters (.210 inches) diameter, a curve of intermediate pressure versus seal clearance for two separate buffer air pressures of 200.7×10^3 N/m^2 (30 psia) and 241.3×10^3 N/m^2 (35 psia) is shown in Figure 3. As shown

in the figure, seal clearance may not exceed 1.27×10^{-3} meters (0.050 inch) and 2.16×10^{-3} meters (0.085 inch), respectively, when a primary air pressure of 172.4×10^3 N/m^2 (25 psia) exists. Should the clearance exceed these values at the stated condition, primary compartment gas will flow through the seal resulting in unfavorable thermal response of the components.

The effect of buffer air temperature on the three seal air flows (W_1, W_2, W_3) when the buffer pressure is held constant at 174×10^3 N/m^2 (30 psia) can be studied in Figures 4, 5, & 6. The changes in seal air flows for different buffer pressures while the buffer air temperature remains constant at 294°K (70°F) are shown in Figures 7, 8, and 9.

As shown in Figures 6 and 9, the primary air flow, W_3, reaches a maximum value then declines with further increases in knife edge clearance. This may be explained by examining Equation 8 and the inter-relationship of its constituents: flow area, A; flow function, ϕ; and intermediate pressure, P_I. As presented in Figure 3, at any given ambient condition at the knife edge, intermediate pressure decreases as the knife edge clearance (flow area, A) increases. This reduction in primary pressure results in the selection of lower values for the flow function, ϕ in Figure 2, as the pressure ratio P_P/P_I increases. The flow function diminishes in value and its non linear rate of change becomes more rapid as the pressure ratio approaches 1.0. In contrast, the flow area is proportional to the knife edge clearance and its rate of change increases at a constant rate as knife edge clearance increases. Therefore, W_3 will arrive at a maximum value then deminish when the rate of change at which the value of ϕ decreases exceeds the constant rate of change in the flow area.

2. Thermal Analysis

Seal design analysis has shown that heat transfer and temperature distribution within the seal are the prime factors affecting seal clearance. A detailed thermal analysis (ref. 3 and 4) indicated that a layer of insulation between the seal stator and the primary gas path is needed to improve clearance control and to aid in preventing overtemperature of the abradable material on the seal stator. The thermal effects of secondary seal design changes were also evaluated. Basic studies to determine the effect of operating conditions on seal temperature distribution were conducted.

Results of the effect of operating conditions on the test seal are presented in Figures 10-13. In Figure 10 the temperature distribution across the stator portion of the seal is shown when an axially translating secondary seal piston ring was employed. The analysis was performed for a primary air temperature of 1033°K (1400°F), a buffer temperature of 450°K (350°F), and an exhaust or ambient temperature of 294°K (70°F). However, the design selected for the contract test program was of resilient sheet metal which allows less heat transfer to the stator than the axially translating piston ring which was analyzed prior to seal design selection. Therefore, the analysis presented here yields a conservative temperature profile.

Figures 11, 12, and 13 relate the changes in stator temperature distribution resulting from changes in seal operating conditions. In Figure 11, buffer air flow to the primary gas path side of the seal has been reduced to zero, allowing 1033°K (1400°F) air to penetrate into the intermediate region of the seal. The average temperature and axial thermal gradient in the stator then increase significantly and the maximum temperature in the abradable material is raised to 732°K (857°F), an increase of over 250°K (450°F). This flow situation, once established, tends to be self-generating because the primary air mixes with buffer air flowing to ambient and causes further thermal growth of the stator.

As seal clearance diminishes, the intermediate pressure increases resulting in a larger ΔP across the knife edges. The gas flow velocities increase correspondingly. Higher heat transfer coefficients result on the stator surfaces exposed to this increase in velocity. However, the change is not as dramatic to the surfaces exposed to ambient gas flows. This is because the percent change in the ambient pressure drop is less than the percent change in the primary pressure drop resulting in a lesser increase in ambient flow velocity than in primary flow velocity. Figure 12 describes the effect of increasing heat transfer film coefficients as indicated on the stator surfaces exposed to buffer air flow in the seal clearance. These decreases in average stator temperature, axial thermal gradient and maximum abradable temperature are all less than 5.6°K (10°F). Figure 13 shows the effect of reducing buffer air temperature to 394°K (250°F). The average stator temperature is reduced by more than 44.4°K (80°F) indicating that the stator temperature level is very sensitive to buffer air temperature. Rotor temperature distributions are shown in Figures 14 and 15. Figure 14 represents the normal operating condition with 450°K (350°F) buffer air while Figure 15 represents a primary air flow reversal condition. The 294°K (70°F) ambient air temperature is the dominant factor in the control of rotor metal temperatures. Rotor displacements caused by these temperature distributions are described in the structural analysis discussion.

3. Structural Analysis

Stresses and deflections in seal stator and rotor components were calculated to predict the effects of pressure, temperature and speed on seal clearance and structural integrity. A generalized analysis for axisymmetric shell structures, with either continuous or periodic loading over the circumference, was programmed for solution on a digital computer (ref. 5).

Figure 16 illustrates the effects of axisymmetric pressure loading and temperature distribution on the seal stator structure. The radial growths indicated in Table I of the following section 4 are accompanied by angular displacements of the stator structure which are caused by axial thermal gradients. The angular displacement causes some degree of clearance variation over the length of the seal which has been neglected in the seal flow analysis.

The effects of pressure, temperature and speed on the rotor structure are shown in Figures 17 and 18. Average radial growth is low because the bulk of the rotor structure is close to ambient temperature. Angular displacements are due to the combined effects of axial thermal gradients and axial pressure loading. The angular displacements of the rotor tend to match those of the stator at a given operating condition.

4. Seal Performance Analysis

The independent effects of gas pressure, temperature, and rotor speed on seal clearance and seal leakage data have been analyzed. Combinations of each of these parameters are now defined and the resulting seal clearances and leakage rates predicted.

The resulting seal clearance at a given operating condition is controlled by thermal growth of both the rotor and stator and also by the elastic growth of the rotor due to speed. Elastic deflections of the rotor or stator due to gas pressure loading were considered to be negligible. Seal pressures, however, may affect seal clearances to a minor degree by altering the heat transfer and temperature distribution within the seal assembly. This effect was not studied in the design analysis. When seal clearance is known, the seal leakage becomes a function of both pressure and temperature. The relative velocity between the rotor and stator surfaces is believed to have little effect on seal leakage at a given seal clearance.

Operating conditions expected in the seal evaluation are presented in Table I. In addition, the analytically calculated seal performance, knife edge clearance and seal air flows are shown. The seal clearance is first calculated from thermal and dynamic conditions. With clearance known, seal air flows are then obtained from the curves in Figures 4-9.

The first condition, Case A, presented in Table I, is a "cold" flow static calibration which provides a check of the effective seal area of both the single and double knife edge seals at assembly. In Case B, the effect of a rotor speed of 6961 rpm on seal clearance and subsequently on seal air flow is presented. The effect of increasing the air temperature of both the buffer and primary air supply 394°K (250°F) and 922°K (1200°F), respectively, on seal air flow is found in Case C. Here, the combined radial growths of both the rotor and stator are considered. Case D defines the effect of further increase in buffer gas temperature to 450°K (350°F) on clearance and seal flow. In Case E, the effect of increasing the ambient air temperature level to 367°K (200°F) is shown.

The final two cases, F&G are repeats of cases A&B respectively except that the buffer air pressure was increased from 200.7 x 10^3 N/m^2 (30 psia) to 241.3 x 10^3N/m^2 (35 psia). At the higher buffer air pressure, the maximum allowable seal clearance is .216 x 10^{-2} meter (.085 inch) as obtained in Figure 3. This value is larger than the maximum expected clearances in Cases C, D, & E. Thus, if the buffer air pressure is maintained at 241.3 x 10^3 N/m^2 (35 psia), the proper sealing flow condition is held for all expected operating clearances.

B. SEAL AND RIG FINAL DESIGN

The final design of the buffered abradable labyrinth seal is functionally similar to the first-stage turbine inner air seal concept for the two-stage tip turbine design as it is shown on NASA-Lewis Research Drawing No. CR 655807. The scheme selected for rig evaluation, and shown in Fig. 19, consists of a rotating knife edge ring mounted on the test rig rotor disk and a stator manifold assembly mounted from the test rig spool case through radial positioning lugs.

1. Principal Seal Features

The labyrinth seal ring, shown in Figure 20, is continuous and incorporates integrally machined knife edges with a tip diameter of 71.12 x 10^{-2} meters (28 inches). The seal ring engages snap diameters on the rotor disk and side plate which closely controls the concentricity of the ring to the rotor. Axial location of the ring is assured by closely controlled tolerances at the butt joints of the related components. The seal ring and other rotor components are machined from AMS 5660 nickel alloy material.

The seal stator assembly, Figure 21, includes the buffer gas manifold, an abradable, rubstrip, and an insulating ring. The abradable material is METCO 601 plasma sprayed coating of aluminum powder filled with polymer particulates. The coating is applied directly to the AMS 5613 manifold I.D. Holes through the I. D. of the manifold permit buffer gas to pass into the intermediate pressure cavity formed by the single and double knife edges with the rub strip. Buffer gas enters the manifold through eight (8) equally spaced fittings around the manifold O.D. to insure uniform internal pressure distribution. The side of the manifold exposed to the primary gas compartment is protected from the high temperature gas by an insulating ring. Concentricity of the buffer gas manifold relative to the knife edge seals is adjusted by four positioning lugs which also support the manifold in the spool case. The lugs are designed to permit free radial growth of the manifold.

2. Rig Description

The primary gas duct and rig secondary seal knife edge are incorporated into a subassembly and welded into the rear case. The duct is a semitoroidal structure with an opening to one side allowing primary gas communication to the vicinity of the test seal. The inside of the duct is insulated to reduce heat losses and to keep the duct walls as cool as practical. Four primary gas inlet fittings are located alternately with and in the same plane as four exhaust ports. Baffles are located between the ports allowing the gas to circulate toward the buffer gas manifold. The rig secondary seal knife edge is riveted to the I.D. of the primary gas duct and is in the same axial plane as the land bolted to the rotor side plate. This secondary seal prevents the impingement of hot gas on the rotor I.D.

An intermediate spool case and front case complete the basic rig layout. The spool case contains the buffer gas manifold concentricity adjustment lugs and supports. Buffer gas supply fitting pass-through holes and hand holes for servicing the proximity probes and adjustment lugs are provided around the circumference of the case.

The front case, which completes the ambient compartment, contains access holes (with covers) by which the labyrinth seal can be visually examined to a limited degree. Measurement of seal gap with feeler gages is also accomplished through these holes. Buffer gas flow to the ambient compartment is exhausted from the rig through fittings in the front case.

The spool case and front case each contain a groove to support metal static seals. The buffer gas manifold is trapped between the two static seals to establish its axial location and provide sealing without restraining the radial growth of the manifold.

C. SEAL PROCUREMENT AND INSPECTION – TASK II

Task II required that the contractor procure the components of the abradable buffered labyrinth seal designed under Task I. Procurement also included one spare labyrinth seal ring, special proximity probes and adapter parts for mounting the seal in the test rig. Modifications to the existing test hardware as defined under Task I also were required. Inspection of the test seal components and test rig modifications were completed in accordance with the contractor's established practice and the inspection was approved by the NASA Project Manager.

D. EXPERIMENTAL EVALUATION – TASK III

The objective of the experimental test program was to flow calibrate a buffered labyrinth seal under environmental conditions similar to those expected at a first-stage lift fan tip turbine inner air seal. The flow calibration of the seal, as a function of knife edge clearance, buffer gas temperature and pressure, and the pressures and temperatures of the ambient and primary gas streams was performed in a thirty-point test program. The data was then used to validate the analytical design system developed under Task I.

1. Facilities and Instrumentation

To provide the various gas flows required, the rig was serviced by the air system shown schematically in Figure 22. Air delivered to the test stand was heated by an alcohol burner and directed, as needed, to the rig primary compartment. Buffer gas was heated by mixing hot gas from the same burner with cold air from a second source. Rotor cooling air was delivered to the rig unheated. All three air supply flows were measured by orifice flowmeters. The buffer gas which flows across the double knife edge was measured by an orifice flowmeter located in the ambient compartment exhaust line. The gas flow across the single knife edge was determined by the difference between the buffered gas supply flow and the ambient exhaust flow. Rig leakage was estimated to be less than the accuracy of the flow measuring devices and, was therefore, considered negligible.

In addition to the gas flows, other measurements include rig compartment air pressures and temperatures, component surface temperatures and radial changes to the seal gap. All of these parameters were measured by conventional sensors. Pressure taps were connected to gages on "U" tubes and chromel-alumel type thermocouple outputs were either recorded automatically or manually from potential type read out devices. Eddy current type proximity probes were used to measure the seal gap and data was recorded from a digital voltmeter and oscilloscope.

The proximity probes were mounted in the buffer gas manifold in radial "pass through" tubes. The probes were threaded into the manifold I.D. end of the tubes, as shown in Figure 19. The head of the probes protruded through holes in the abradable rubstrip and measured the distance to the platform between the two widest spaced knife edges. This arrangement minimized errors due to differential thermal expansion between the buffer gas manifold and the proximity probes. The probes were statically temperature calibrated before installation and displacement calibrated statically after installation into the rig. The rig, assembled and installed in the test cell, is shown in Figure 23.

2. Build 1 Seal Testing with Static Cold Clearances of $.127 \times 10^{-2}$ Meter (.050 Inch)

The test seal as it was installed in the rig is shown in Figure 24. The buffer gas manifold was adjusted to establish an average knife edge gap of $.124 \times 10^{-2}$ meter (.049 inch). Testing was initiated following the 15 point program shown in Table II.

The first six points were obtained at static (no speed) conditions with room temperature air. Points 1 through 3 were designed to obtain the variation of flow as a function of the

pressure ratio, P_I/P_P, across the single knife edge which separates the intermediate pressure cavity from the primary gas compartment. Primary gas pressure, P_P, was set and measured directly. Intermediate pressure was measured by sealing the ambient compartment (no flow) and measuring that pressure (P_A) which would be the same as P_I. Similarly, points 4 through 6 were designed to obtain the variation of flow as a function of the pressure ratio, P_I/P_A, across the double stage knife edge labyrinth segments that separate the intermediate pressure cavity from the ambient compartment. While these test points were recorded, the primary gas compartment was sealed ($P_P = P_I$) and the ambient compartment was vented to atmosphere, $P_A = 101.4 \times 10^3$ N/m^2 (14.7 psia). The results of points 1 – 3 are shown in Fig. 25 and points 4 through 6 are shown in Figure 26. By measuring P_I in the above manner, the pressure drop through the buffer gas manifold orifice holes could be determined and the flow coefficient through the orifice holes could be calculated. Analysis of the static test results indicated that the flow coefficient for the buffer gas orifices should be 0.8 rather than the predicted value of 0.6 from the Design Analysis. A static flow calibration of the orifices is presented in Figure 27. Based on the pressure drops across the single and double stage labyrinth seal, the analytically calculated uni-directional flows across the seals were found to be in close approximation to the measured values at these pressure drops.

Dynamic points 7 through 12 were run at a constant rig speed of 3480 rpm. Buffer gas pressure and temperature were varied to calibrate the buffer gas as it splits and flows across the single and double stage labyrinths. The primary gas compartment was maintained at approximately 170.3×10^3 N/m^2 (24.7 psia). The ambient compartment pressure was minimized to the capability of the exhaust plumbing, less than 122.0×10^3 N/m^2 (17.7 psia) at the higher flows. At test points 13 and 14, primary gas, which in previous points was heated only as a result of mixing with the buffer gas, was heated to approximately 922°K (1200°F). Point 15 was a static test point and provided a flow calibration at a $.127 \times 10^{-2}$ meter (0.050 inch) knife edge gap. The results of the above test points are tabulated in Table II.

The calculated flows in Table II were determined by using the measured knife edge gap during the test and with the orifice flow coefficient of 0.8 derived from the six (6) static, unidirectional calibration test points.

At the completion of the first fifteen (15) test points, the buffer gas manifold was removed and examined. Debris suspended in the buffer gas air supply left witness markings, shown in Figure 28, indicating uniform flow distribution from the orifice.

No damage was noted to either the rubstrip or to the labyrinth seal. The abradable material was machined off and the manifold was recoated. The recoated abradable material was machined to provide a nominal $.061 \times 10^{-2}$ meter (0.024 inch) gap with the knife edges.

3. Build 2 Seal Testing With Static Cold Clearance of $.061 \times 10^{-2}$ Meter (.024 in.)

The recoated buffer gas manifold was reinstalled in the rig and adjusted to establish an average knife edge gap of $.061 \times 10^{-2}$ meter (.024 inch). The rotor runout, as measured by the proximity probes, was approximately $.0051 \times 10^{-2}$ meter (.002 inch). The continuation of the test program followed the schedule shown in Table III.

The first six static points were run in the same manner as in previous testing. The flow calibration across the single labyrinth is presented in Figure 29 and the calibration across the two stage labyrinth is presented in Figure 30. Figure 31 is a flow calibration of the orifice holes.

Dynamic points 22 through 24 were run at a constant rig speed of 3480 rpm. Buffer gas pressure and temperature were varied to calibrate the buffer gas as it splits and flows across the single and double stage labyrinths. The primary gas compartment was maintained at approximately 186.1 x 10^3 N/m^2 meters (27 psia). The ambient compartment was minimized to the capability of the exhaust plumbing, less than 110.3 x 10^3 N/m^2 (16 psia) at the higher air flows. At test points 25 through 29, the primary gas, which in previous points was heated only as a result of mixing with the buffer gas, was heated to approximately 922°K (1200°F). At the same time the rig speed was increased to approximately 6000 rpm (5000 at point 25). While attempting to set test point 26, three of the four proximity probes failed from an apparent rub. Survival of one of the probes indicated that the manifold was eccentric to the rotor at this time since all probes were initially set at the same static displacement from the rotor. Point 30 was a static test point and provided a flow calibration at .061 x 10^{-2} meter (.024 inch) seal gap.

At the completion of the test program, the rotor runout, as measured by the proximity probe, was found to be approximately .0051 x 10^{-2} meter (.002 in.) while the seal gap was measured at .0599 x 10^{-2} meter (.0236 inches) average. The manifold was then removed from the rig and the seal components were examined. Grooves in the rub strip caused by the knife edges were evident. The rub was not a full 360° nor was the depth of the penetration symmetrical about the vertical axis indicating that the manifold became out of round and eccentric to the rotor. The maximum depth of the grooves was .076 x 10^{-2} meter (.030 inch). The only wear noted on the knife edges was some rounding off of the edges.

Results of the dynamic testing at the reduced clearance are presented in Table III along with the analytically calculated values.

4. Analysis of Experimental Evaluation

Tables II and III present the seal air flows measured during the dynamic test portion of the seal evaluation for each test condition set. In addition, for each of these test combinations, the predicted air flows are presented for comparison along with the measured parameters used in calculating these flows. To further demonstrate the correlation between test and analytical seal air flows, six (6) test points from Tables II and III were plotted on the analytically generated curves shown in Figures 32, 33, and 34. Data for the analytical curves was obtained from measured compartment pressures and temperatures. Data from the first build with the 1.27 x 10^{-3} meter (.050 inch) cold gap clearance is shown by curves 7, 9, and 11 while data for the second build with the .61 x 10^{-3} meter (.024 inch) cold gap clearance is presented by curves 22, 23, and 24.

As shown in Figure 32, good correlation between the analytical and measured buffer air flows is demonstrated for the larger cold gap clearance. Measured buffer flows at the

reduced cold gap clearance, however, do not fall as close to the analytical curves. It should be noted that at the smaller seal clearance the knife edge discharge coefficient (α) varies more for small deviations in clearance than it does at the larger clearance (Figure 2). Therefore, small differences between actual and measured clearance would have a greater effect on the relationship between analytical and experimental air flow at the smaller clearance.

In addition, the effect of the knife edge tip radius on the flow coefficient is not known and, therefore, was not used in the analytical computation. With the present system, the buffer air flow at the lower seal clearances can be predicted within 20 percent of the experimentally measured flows. To obtain accuracy in the 7 percent range as demonstrated with the larger clearance, greater accuracy in determining the knife edge discharge coefficient is needed.

Figures 33 & 34, demonstrate the correlation between measured and calculated ambient and primary seal air flows at the same conditions considered in Figure 32. Predicted ambient air flows are consistently higher than measured values, whereas, predicted primary flows fall lower. Referring back to Figures 25 and 26, excellent correlation was found between the analytical and measured flows during static calibrations. With a lower ambient flow, the actual primary flow is consequently higher. Referring back to Tables II and III, the flow split across the knife edges for any measured orifice flow is in the range of 10 to 13 percent.

Prediction of seal operating clearance was not as expected. Measured values consistently averaged lower than predicted clearances. Initially, when predictions were made, it was assumed that the rotor could be cooled and maintained below 311°K (100°F). However, in meeting primary air temperature requirements, the rotor cooling air was insufficient to maintain the rotor temperature at the expected level, therefore, resulting in larger thermal rotor growth and thus lower seal gaps. These rotor temperature measurements are documented in Figure 35 and Table IV of Appendix I.

REFERENCES

1. Eshbach, O. W. *"Handbook of Engineering Fundamentals, 2nd Edition,* John Wiley & Sons, Inc., New York, New York

2. Egli, A. *"The Leakage of Steam Through Labyrinth Seals,"* ASME Transactions, Vol. 57, 1935.

3. Eckert, E. R. and Drake, R. M., Jr. *"Heat and Mass Transfer,"* Mc Graw - Hill Book Co., New York, New York, 1959

4. Kreith, F. *"Principles of Heat Transfer"* Second Edition, International Textbook Co., Scranton, Pennsylvania.

5. Roark, R. J. *"Formula For Stress and Strain"* third edition, McGraw-Hill Book Co., Inc.

6. Kalnins, A. *"Analysis of Shell Revolution Subject to Symmetrical and Non Symmetrical Loads,"* Journal of Applied Mechanics, Sept. 1964.

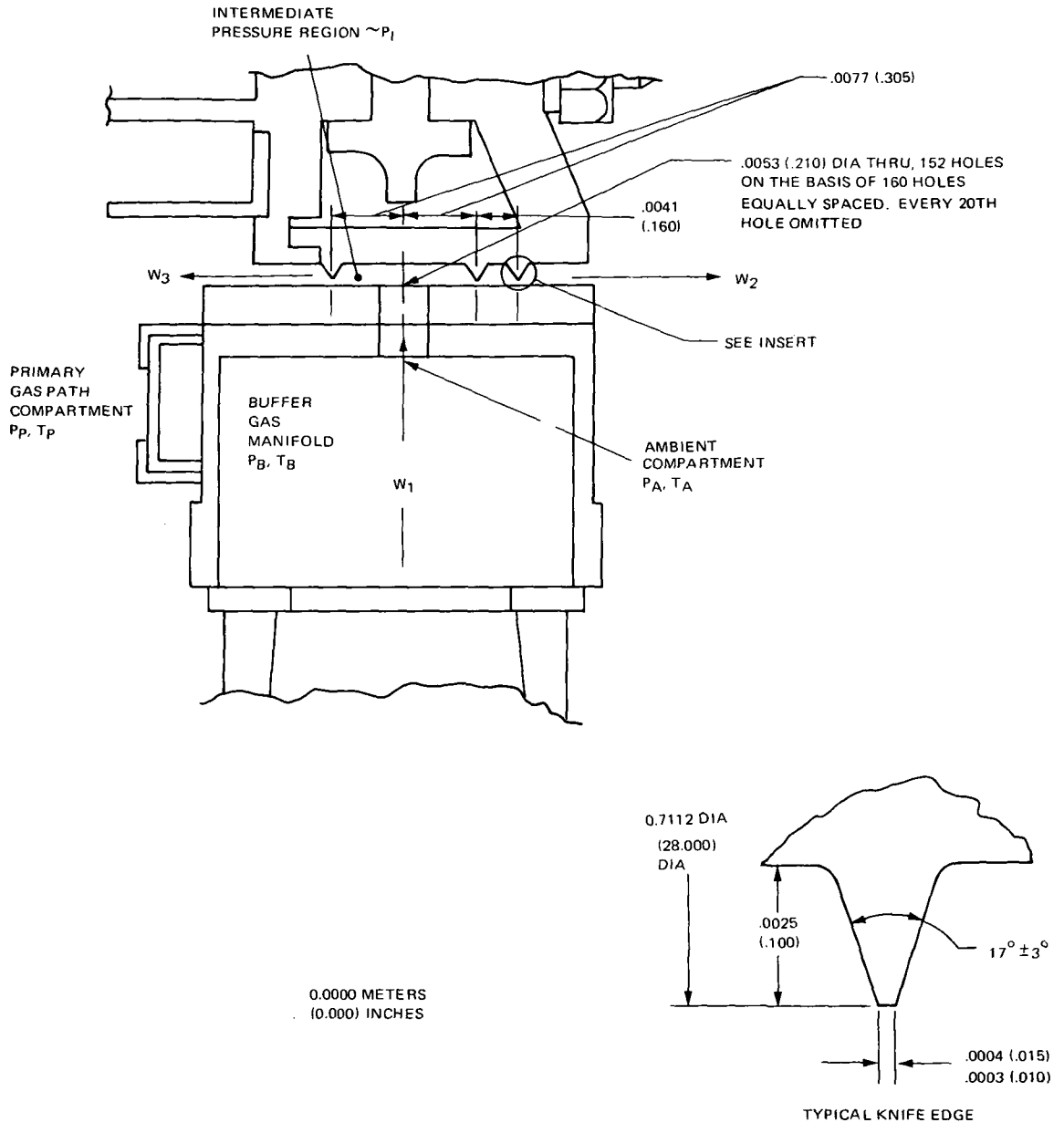

Figure 1 Test Seal Configuration With Flow Paths

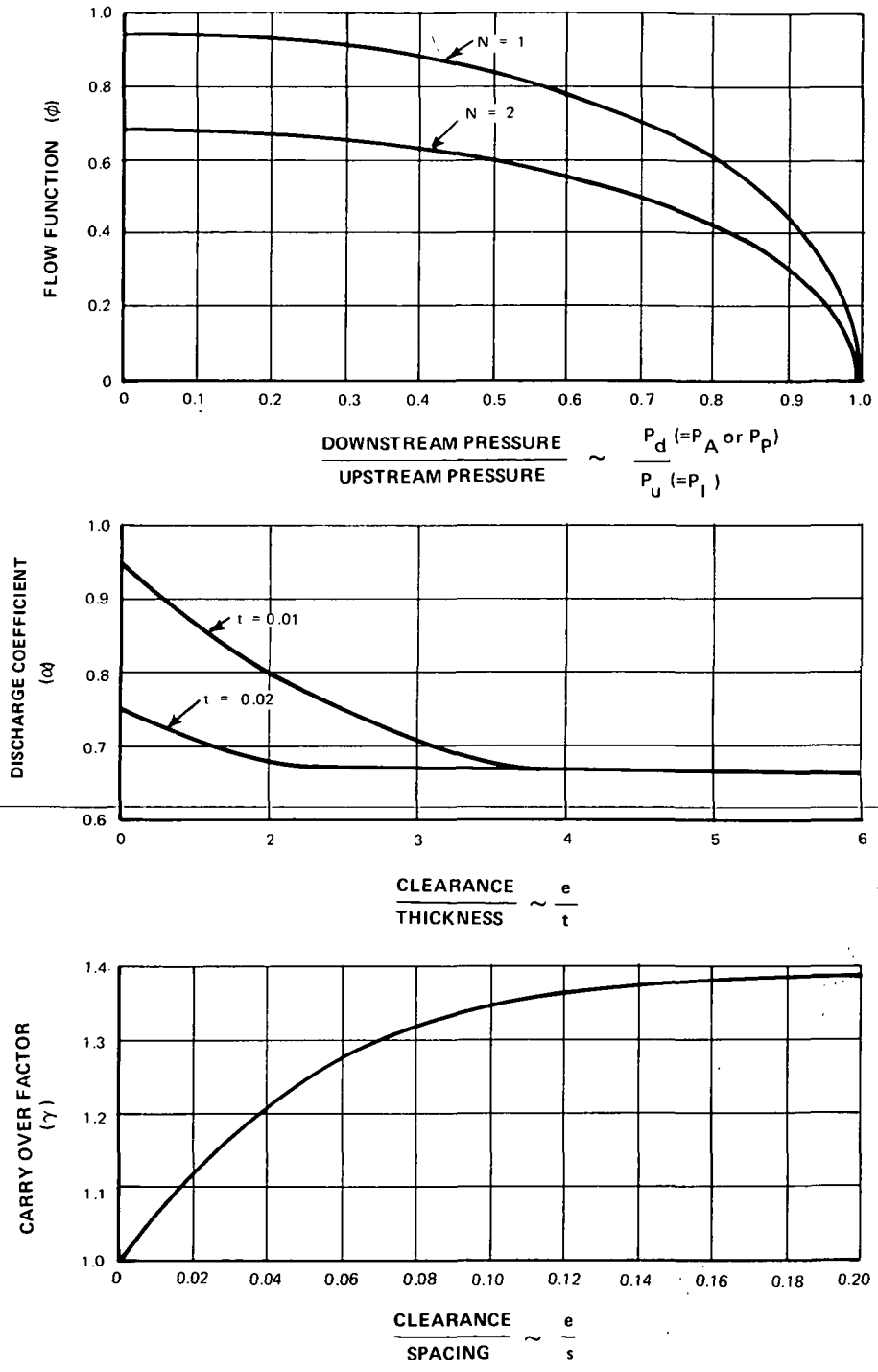

Figure 2 Egli Equation Flow Parameters

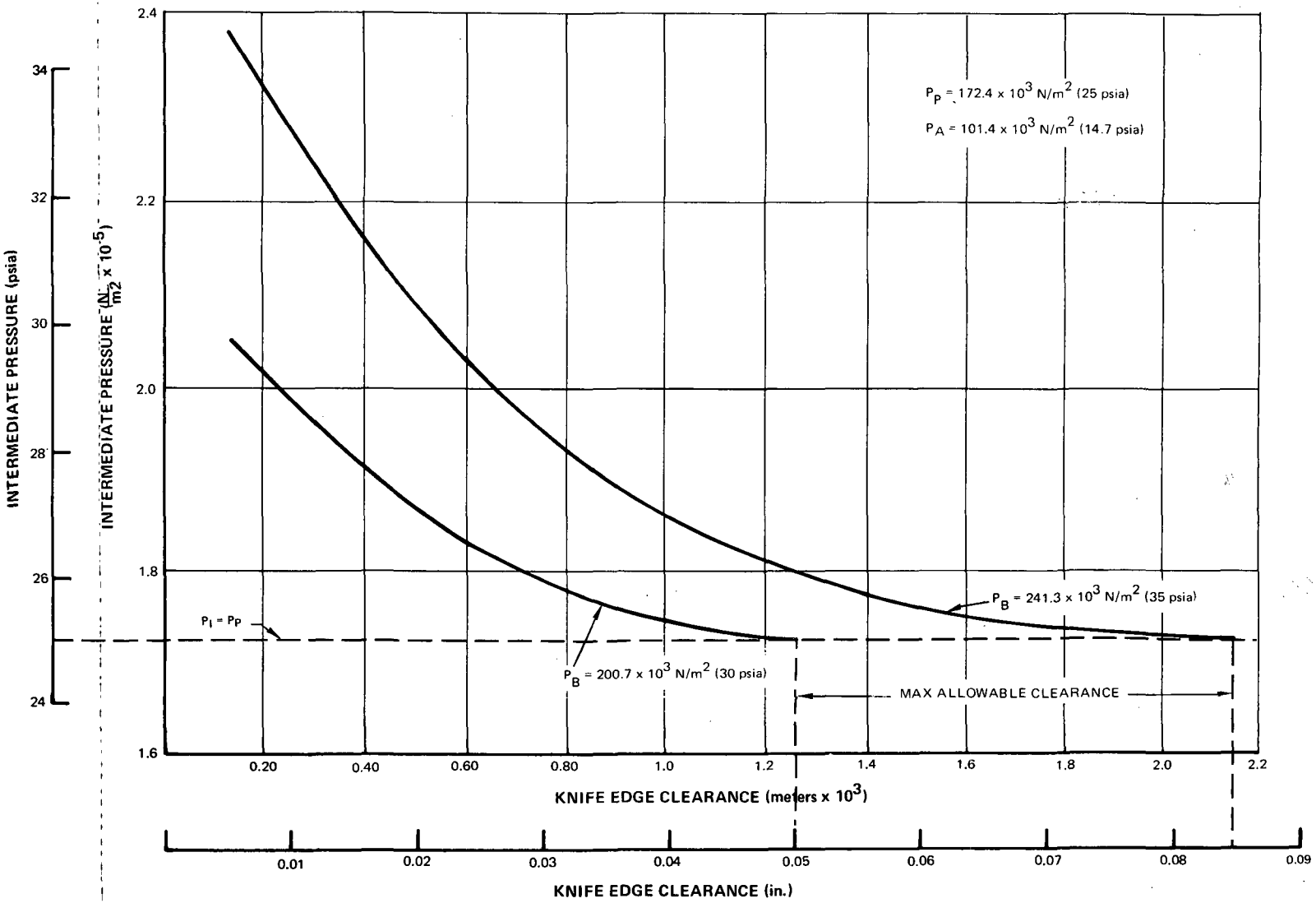

Figure 3 Intermediate Pressure vs. Knife Edge Clearance

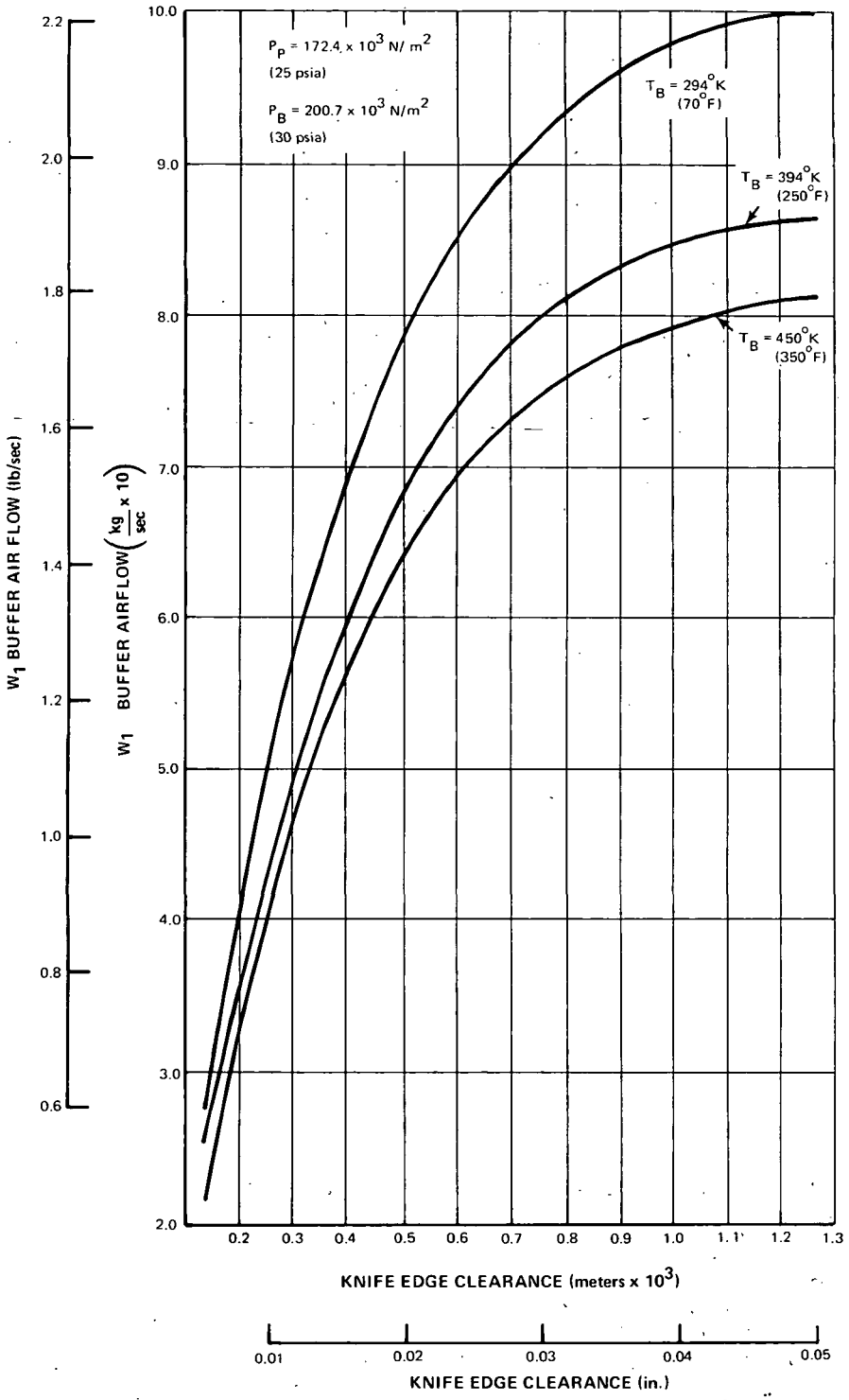

Figure 4 W_1 Buffer Air Flow vs. Clearance

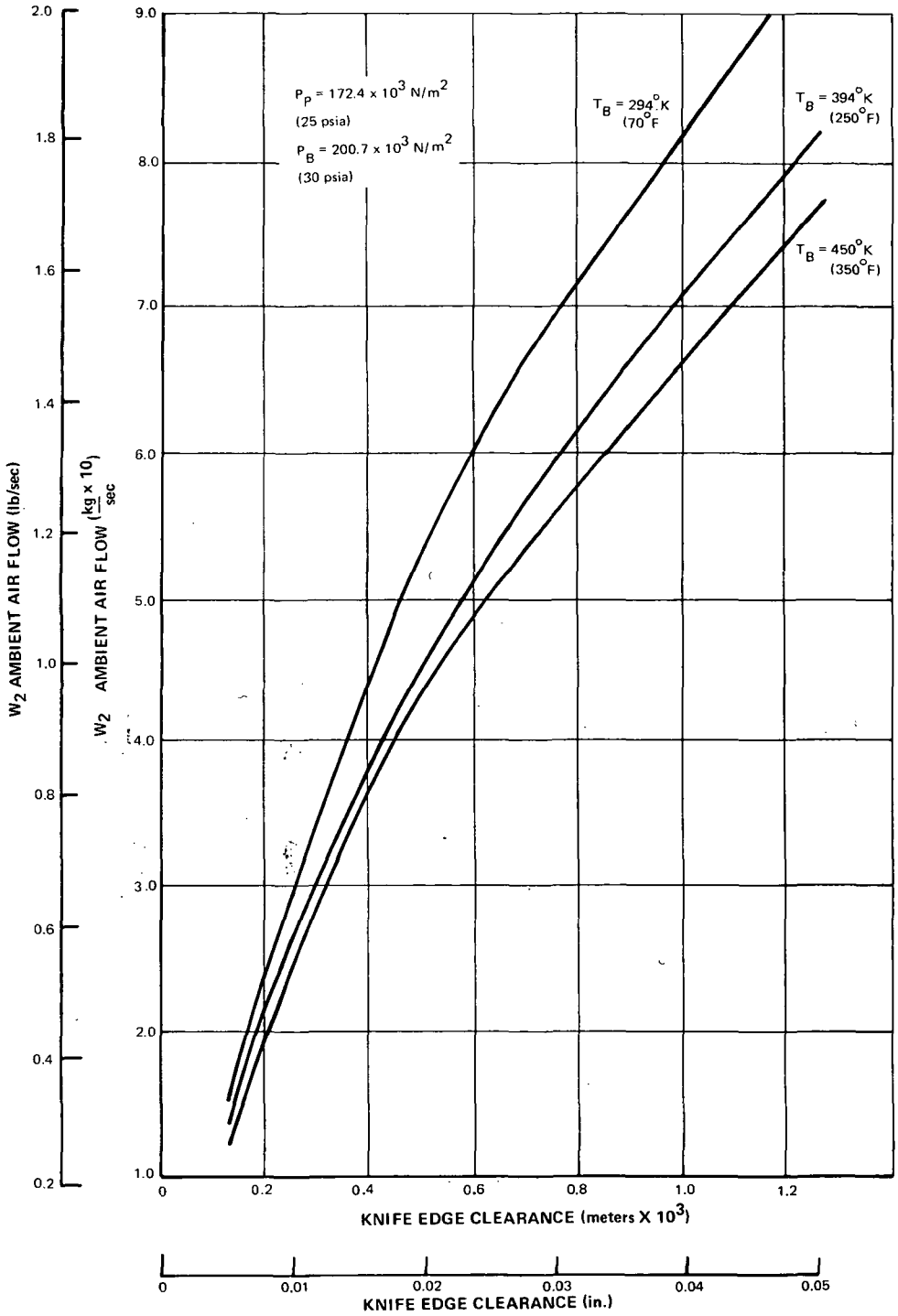

Figure 5 W_2 Ambient Air Flow vs. Clearance

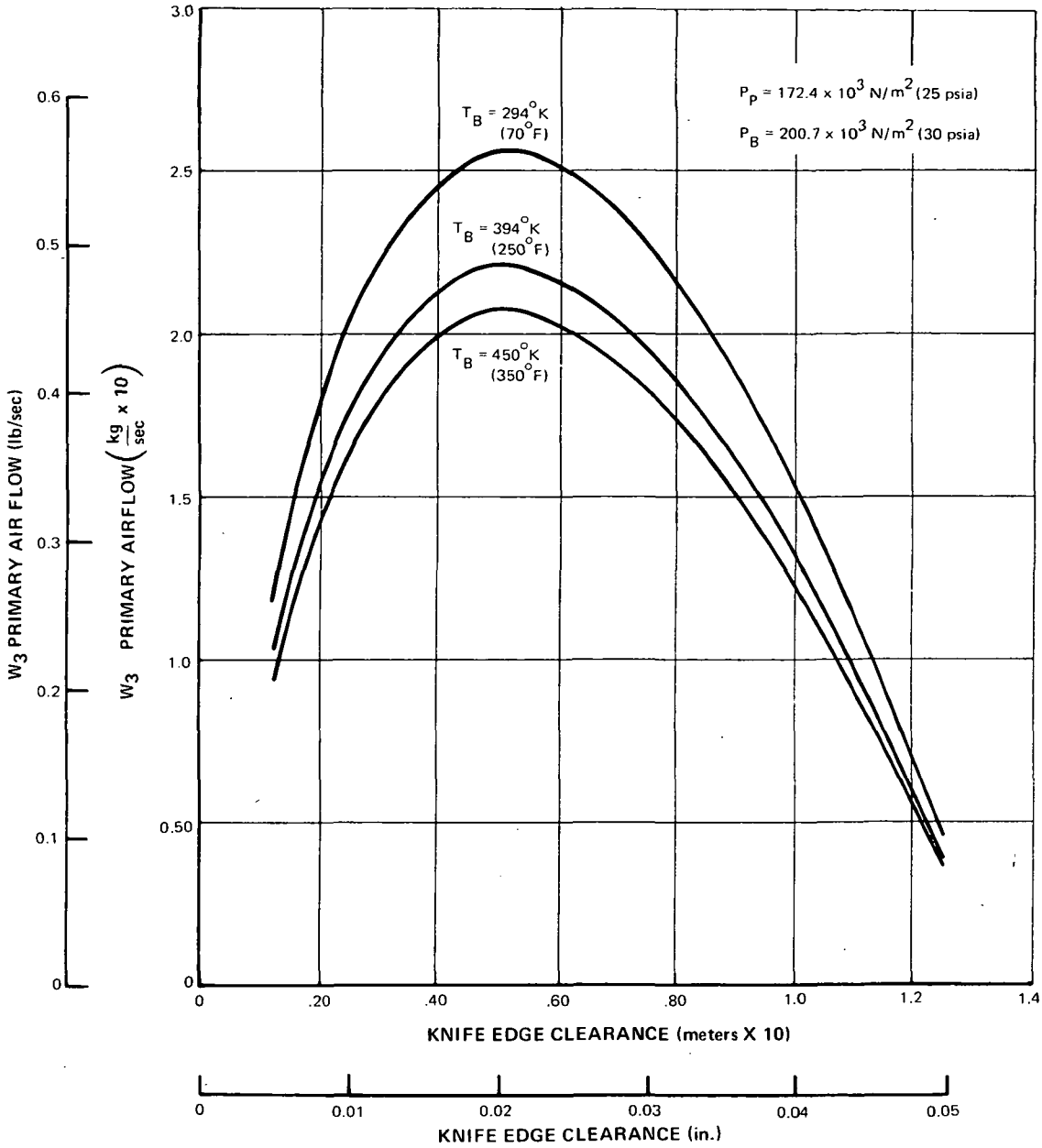

Figure 6 W_3 Primary Air Flow vs. Clearance

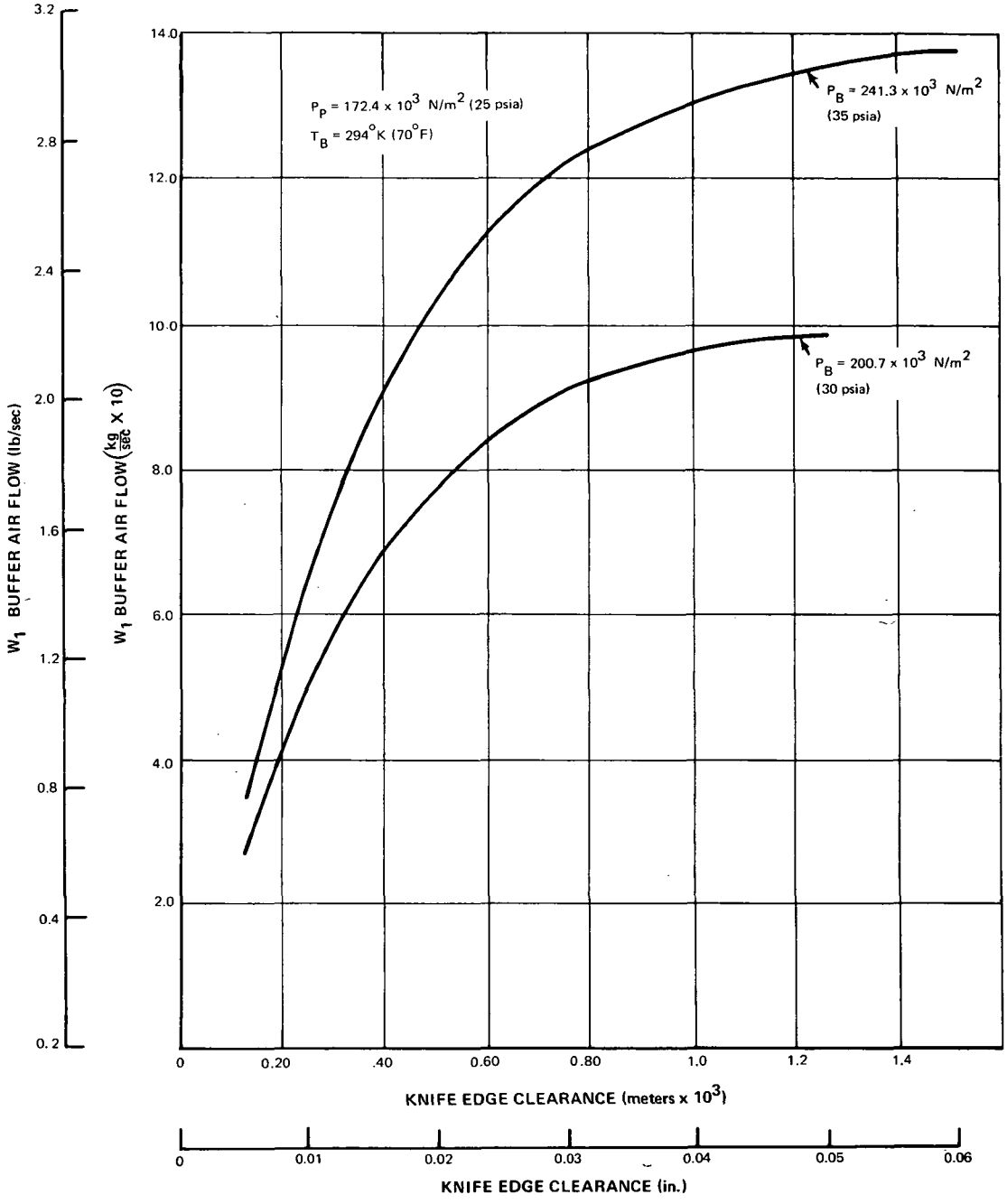

Figure 7 W_1 Buffer Air Flow vs. Clearance

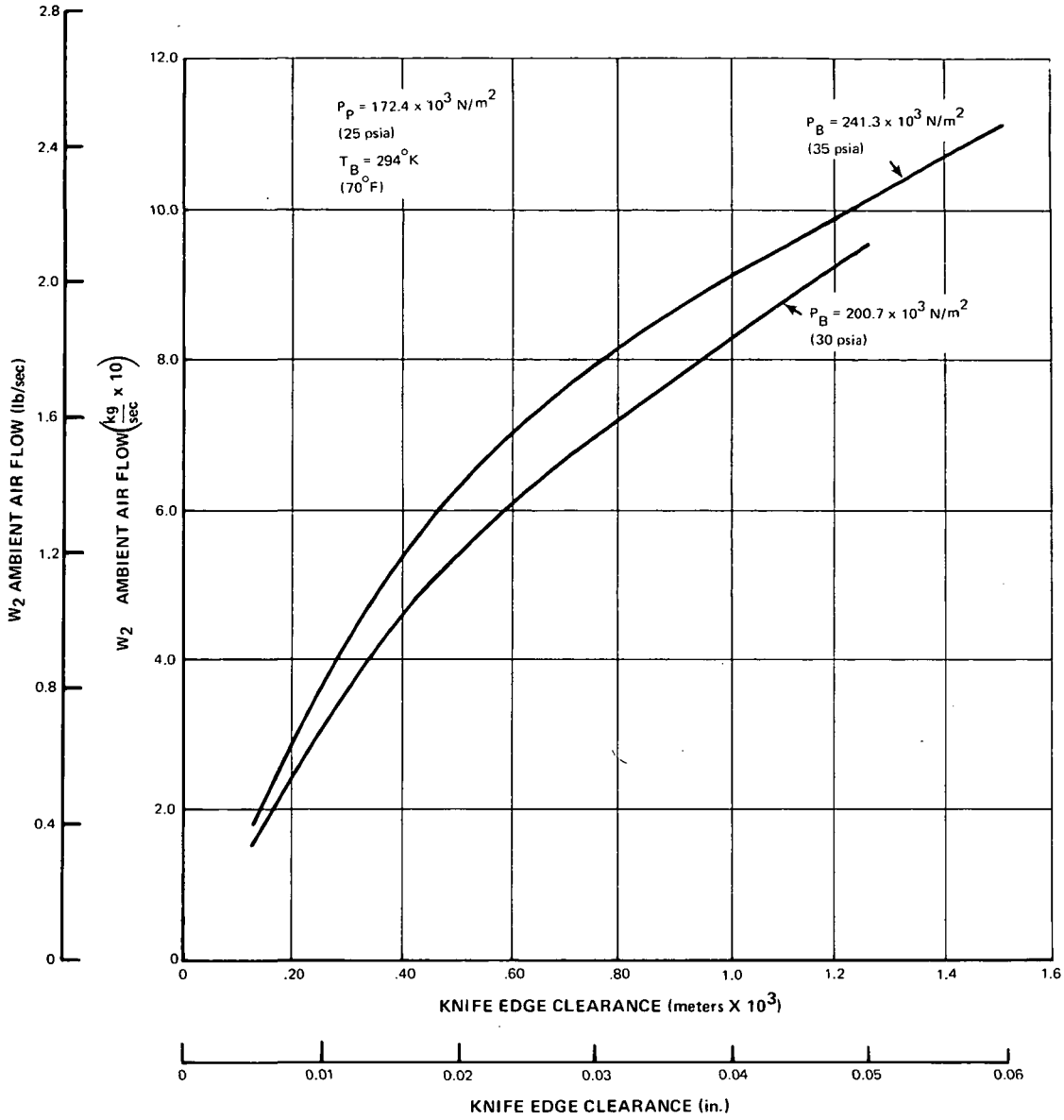

Figure 8 W_2 Ambient Air Flow vs. Clearance

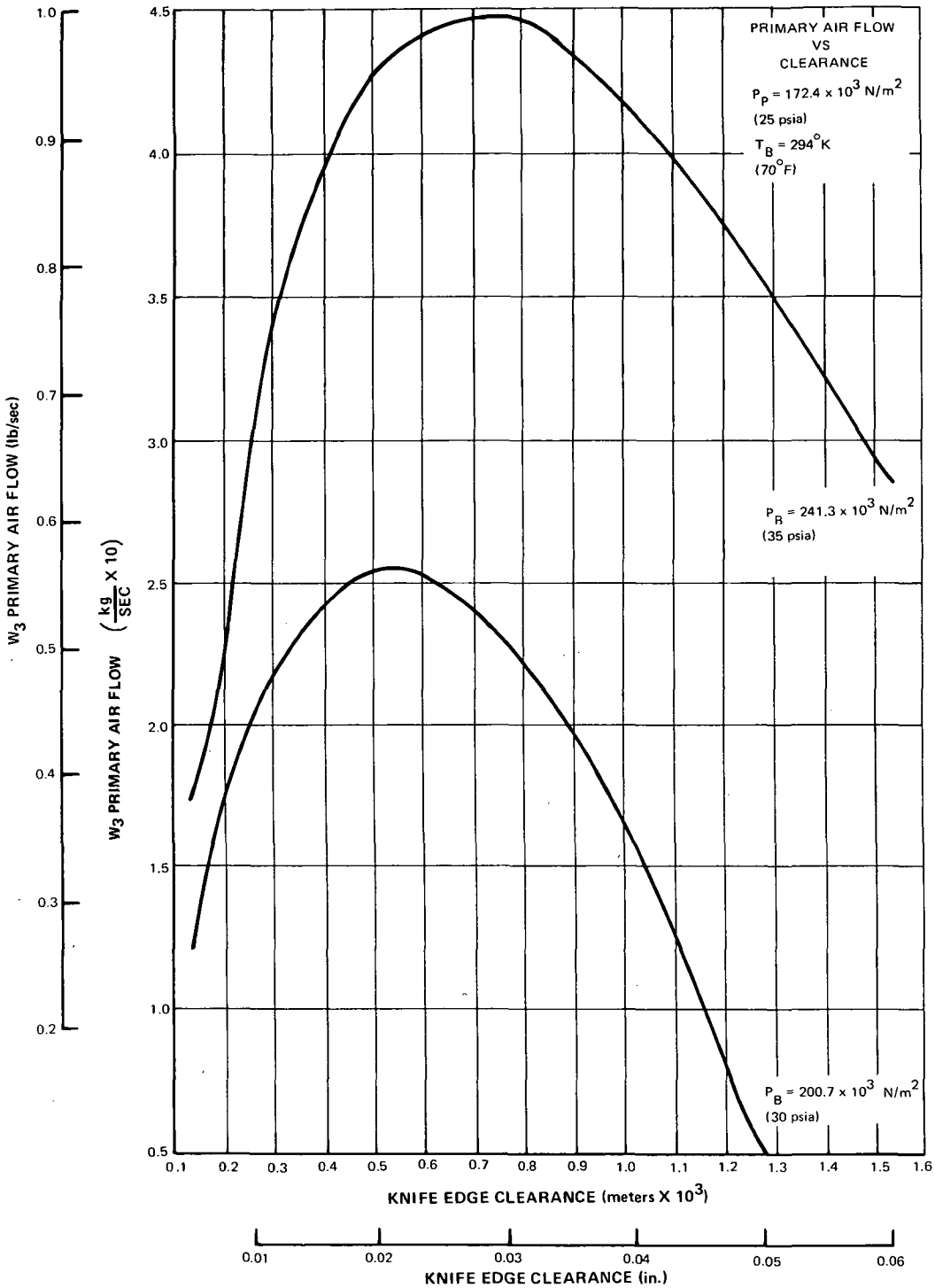

Figure 9 W_3 Primary Air Flow vs. Clearance

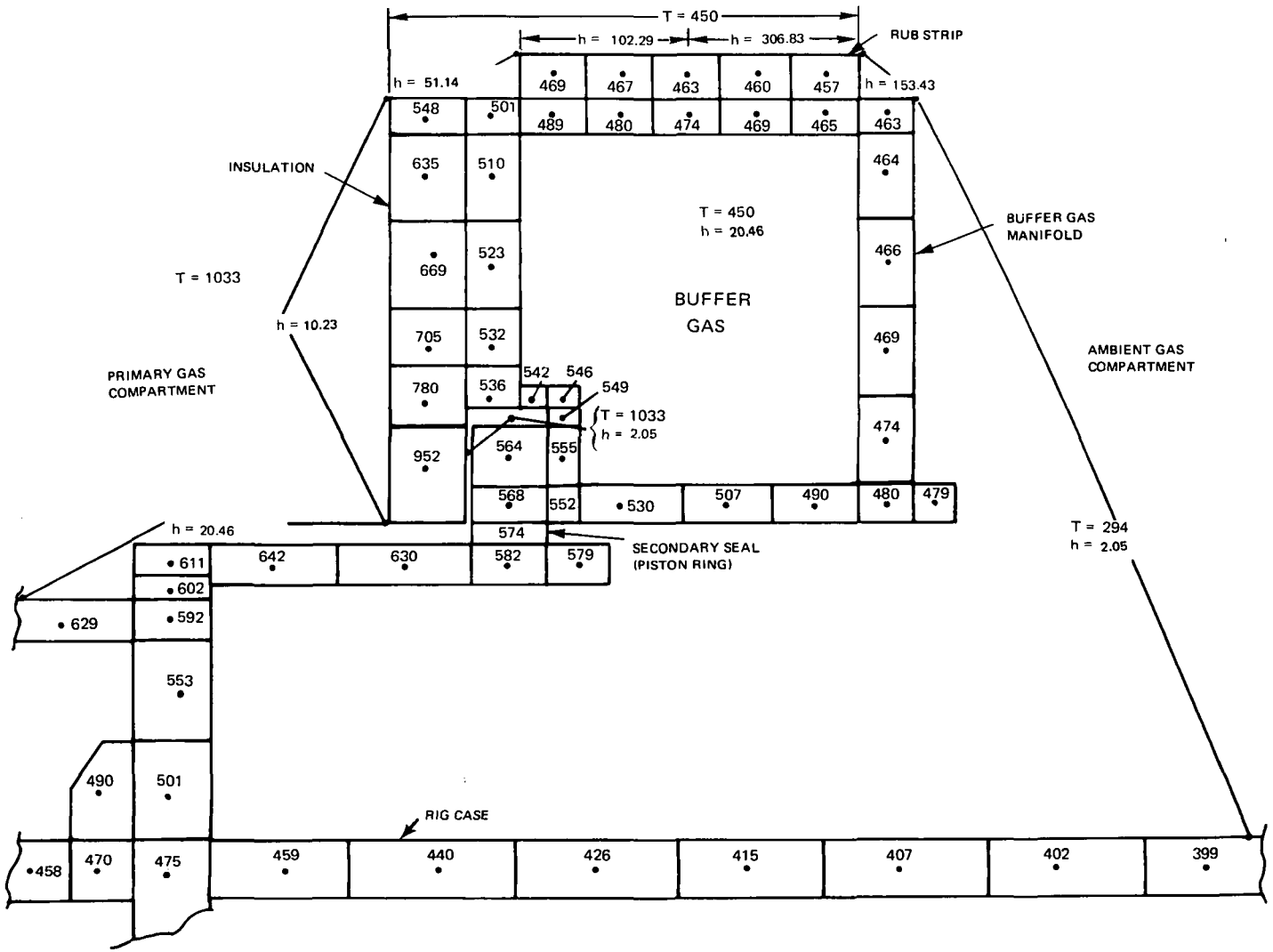

Figure 10 Seal Stator Temperature Distribution At Normal Operation Conditions - SI Units: $T \sim {}^{\circ}K$, $h \sim \frac{\text{joules}}{\text{hr m}^2{}^{\circ}K} \times 10^{-4}$

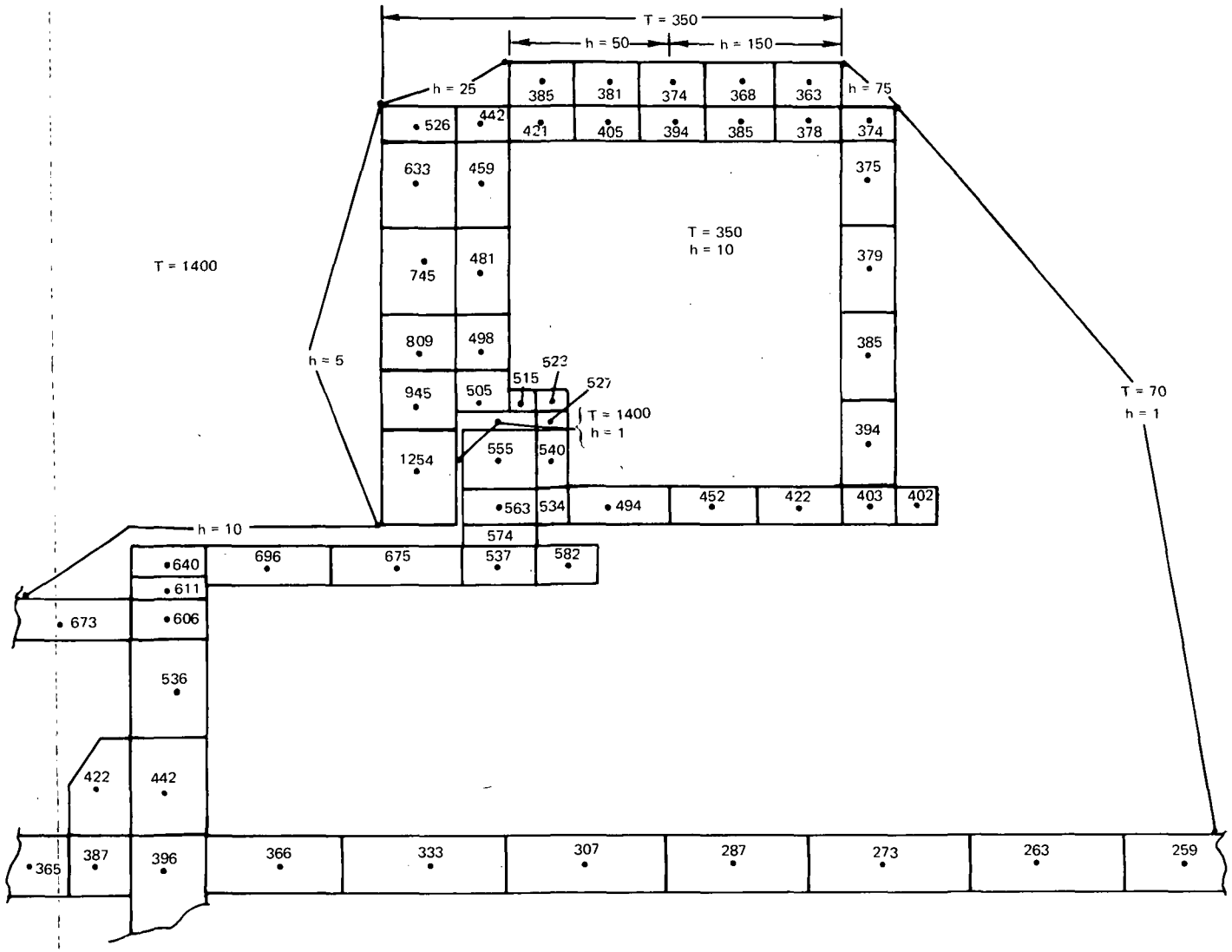

Figure 10A Seal Stator Temperature Distribution At Normal Operating Conditions-
English Units: T~ °F, h~ $\frac{\text{BTU}}{\text{hr ft}^2\,°\text{F}}$

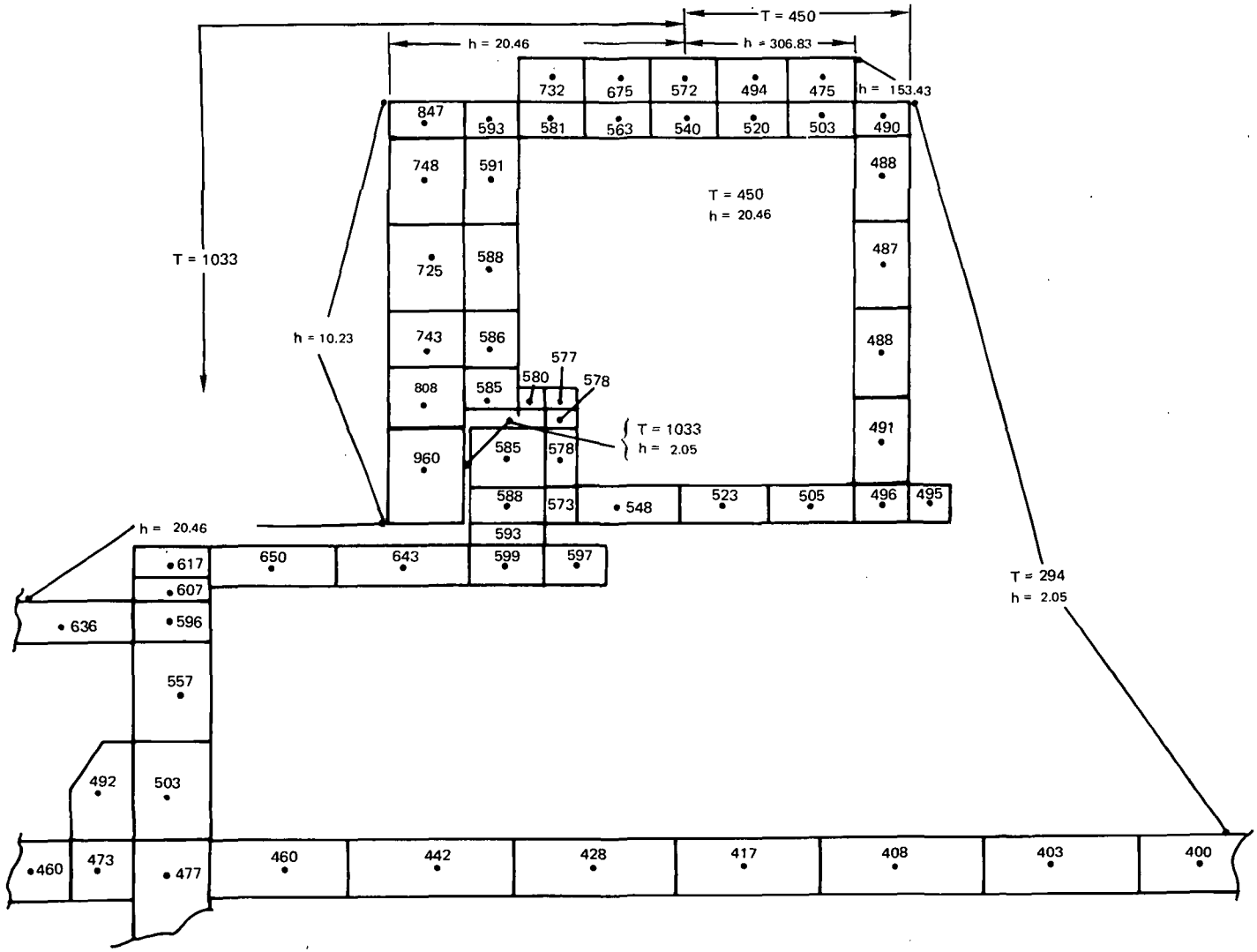

Figure 11 Seal Stator Temperature Distribution With No Buffer Flow to Primary - SI Units $T \sim {}^\circ K$, $h \sim \frac{\text{joules}}{\text{hr m}^2\ {}^\circ K} \times 10^{-4}$

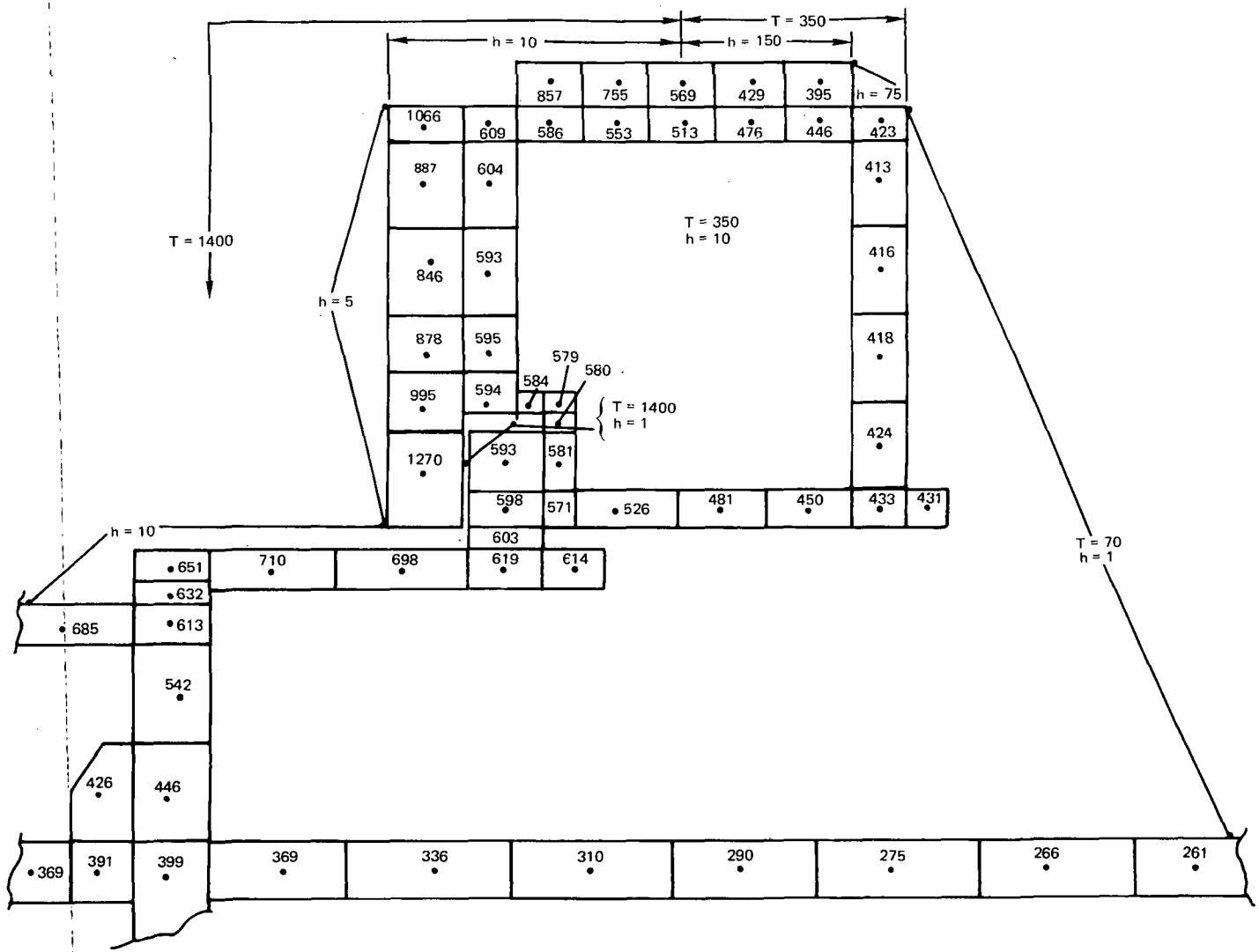

Figure 11A Seal Stator Temperature Distribution With No Buffer Flow to Primary - English Units: T~ °F, h~ $\frac{\text{Btu}}{\text{hr ft}^2\,°\text{F}}$

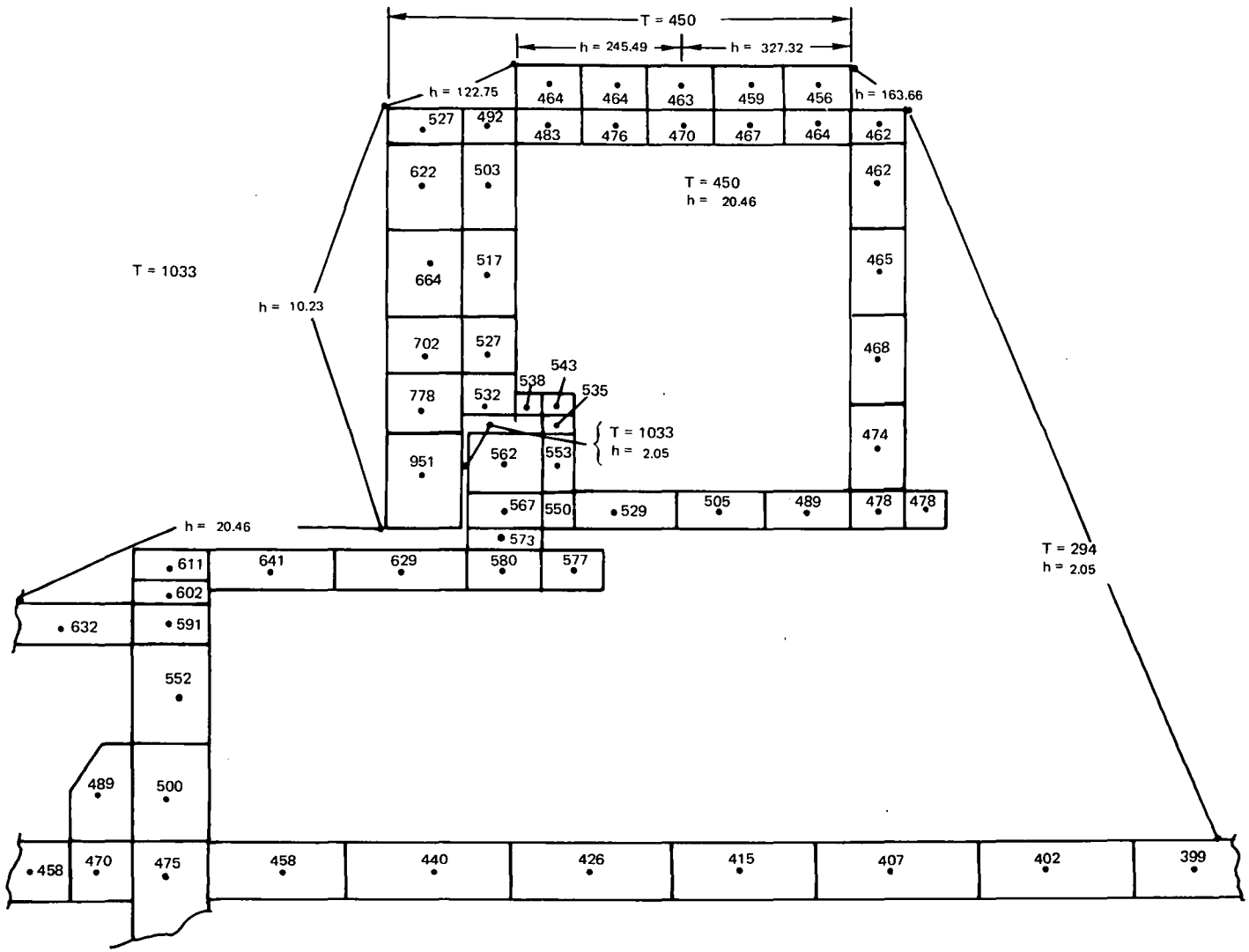

Figure 12 Seal Stator Temperature Distribution With Increased Heat Transfer Coefficients - SI Units: T~ °K, h~ $\frac{\text{joules}}{\text{hr m}^2\,°\text{K}}$ x 10^{-4}

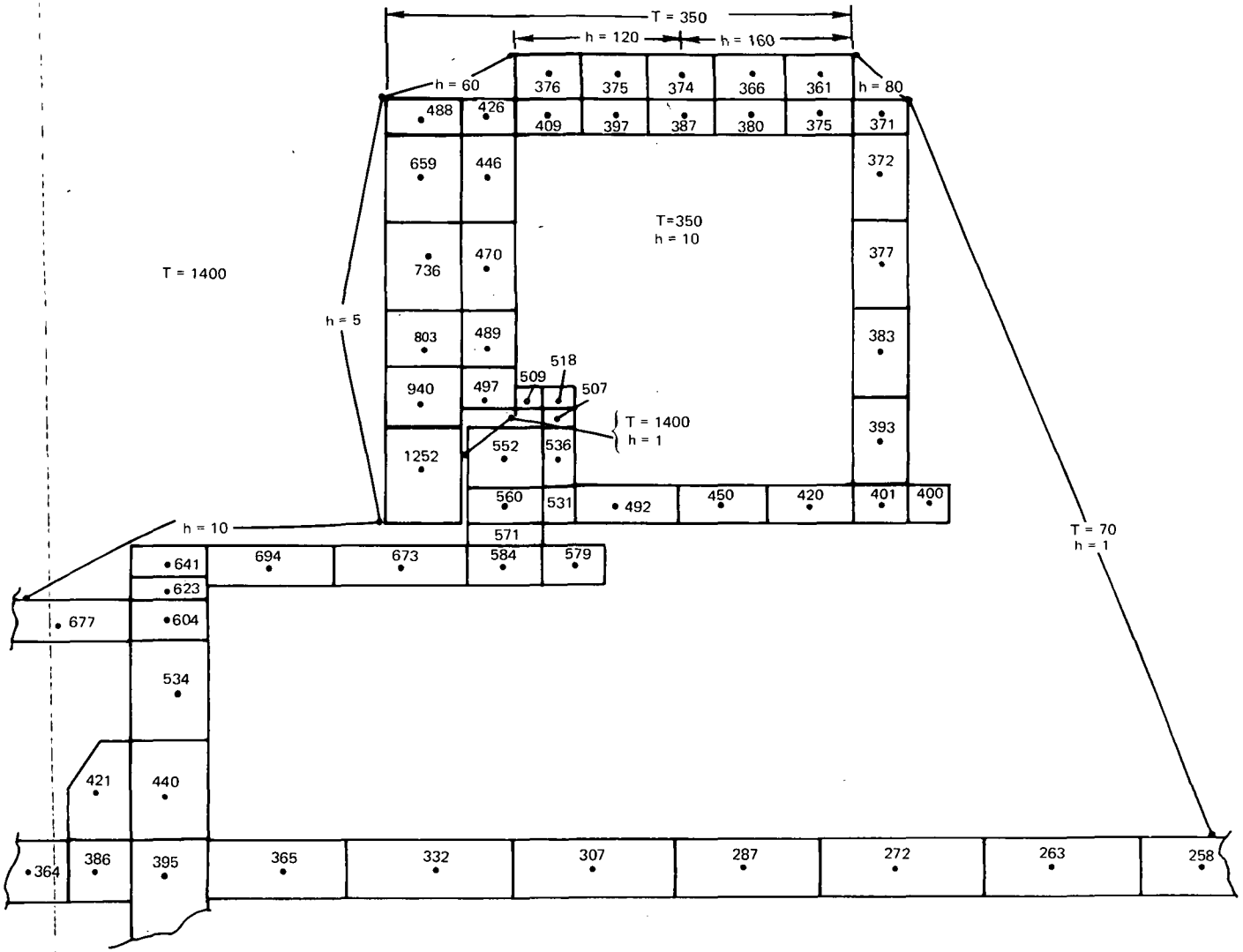

Figure 12A Seal Stator Temperature Distribution With Increased Heat Transfer Coefficients - English Units: $T \sim {}^{\circ}F, h \sim \frac{Btu}{hr\ ft^2 {}^{\circ}F}$

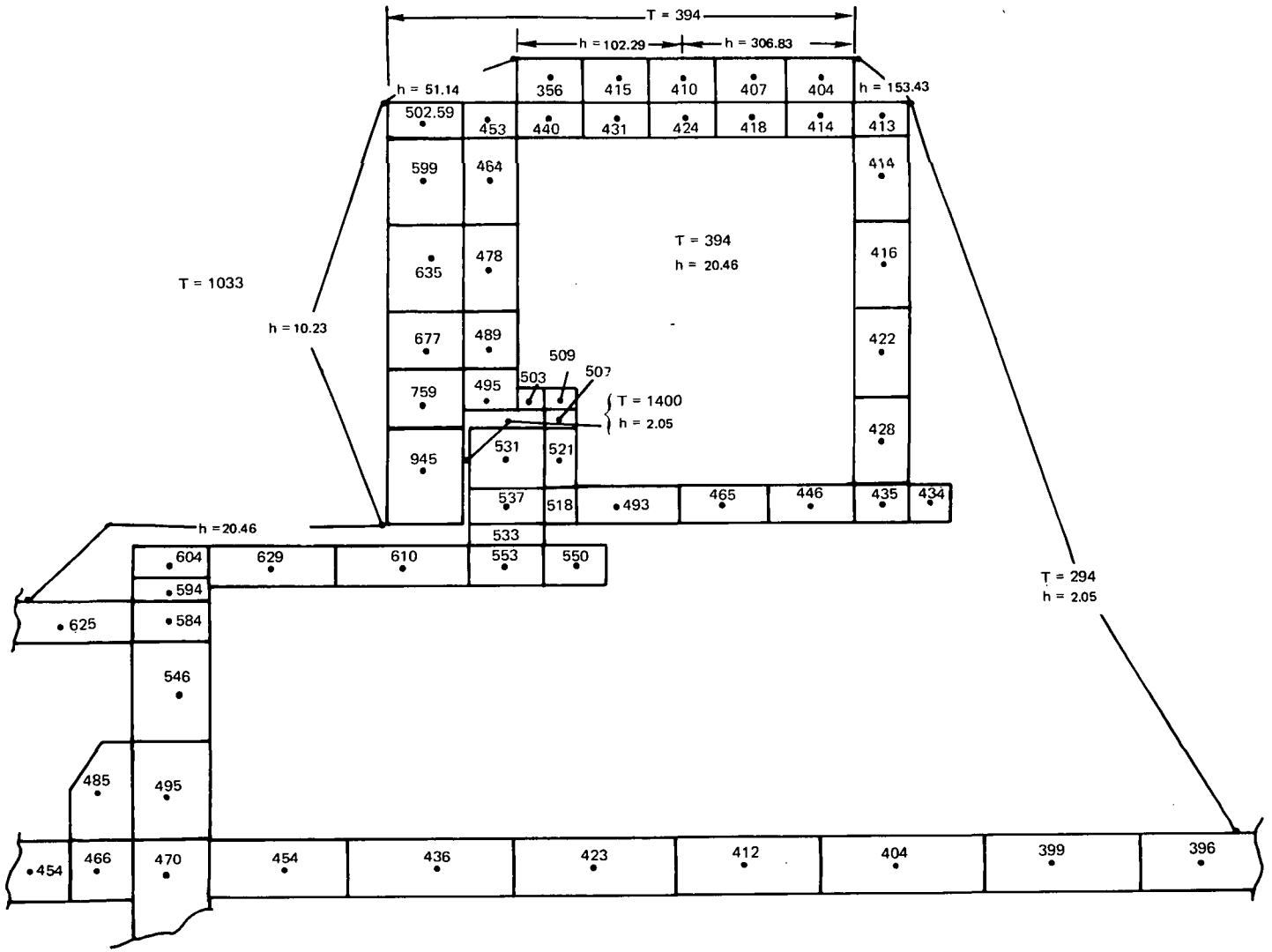

Figure 13 Seal Stator Temperature Distribution With Reduced Buffer Air

Temperature - SI Units: $T \sim {}^{\circ}K, h \sim \frac{\text{joules}}{\text{hr m}^2{}^{\circ}K} \times 10^{-4}$

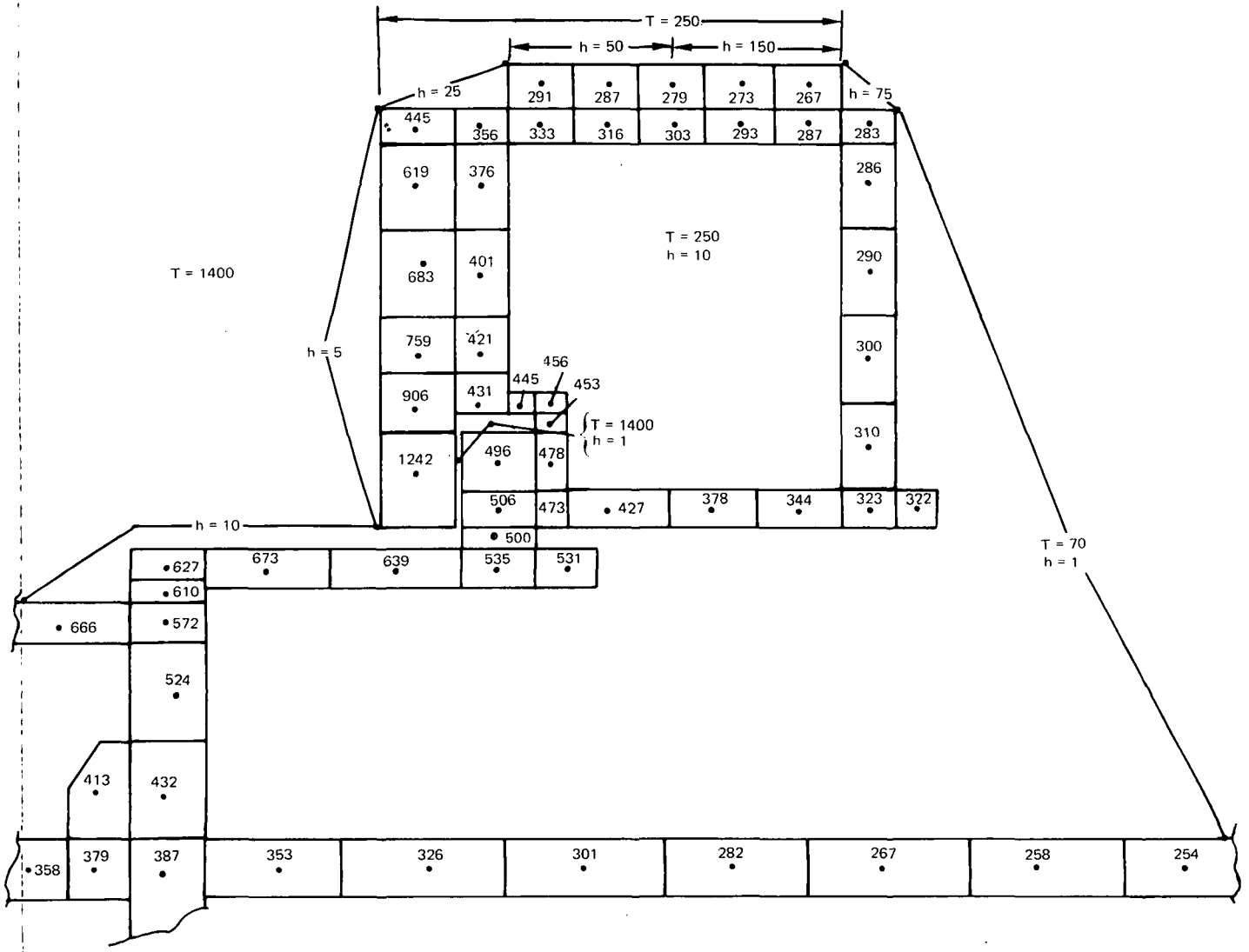

Figure 13A Seal Stator Temperature Distribution With Reduced Buffer Air Temperature - English Units: $T \sim {}^{\circ}F$, $h \sim \frac{Btu}{hr\ ft^2 {}^{\circ}F}$

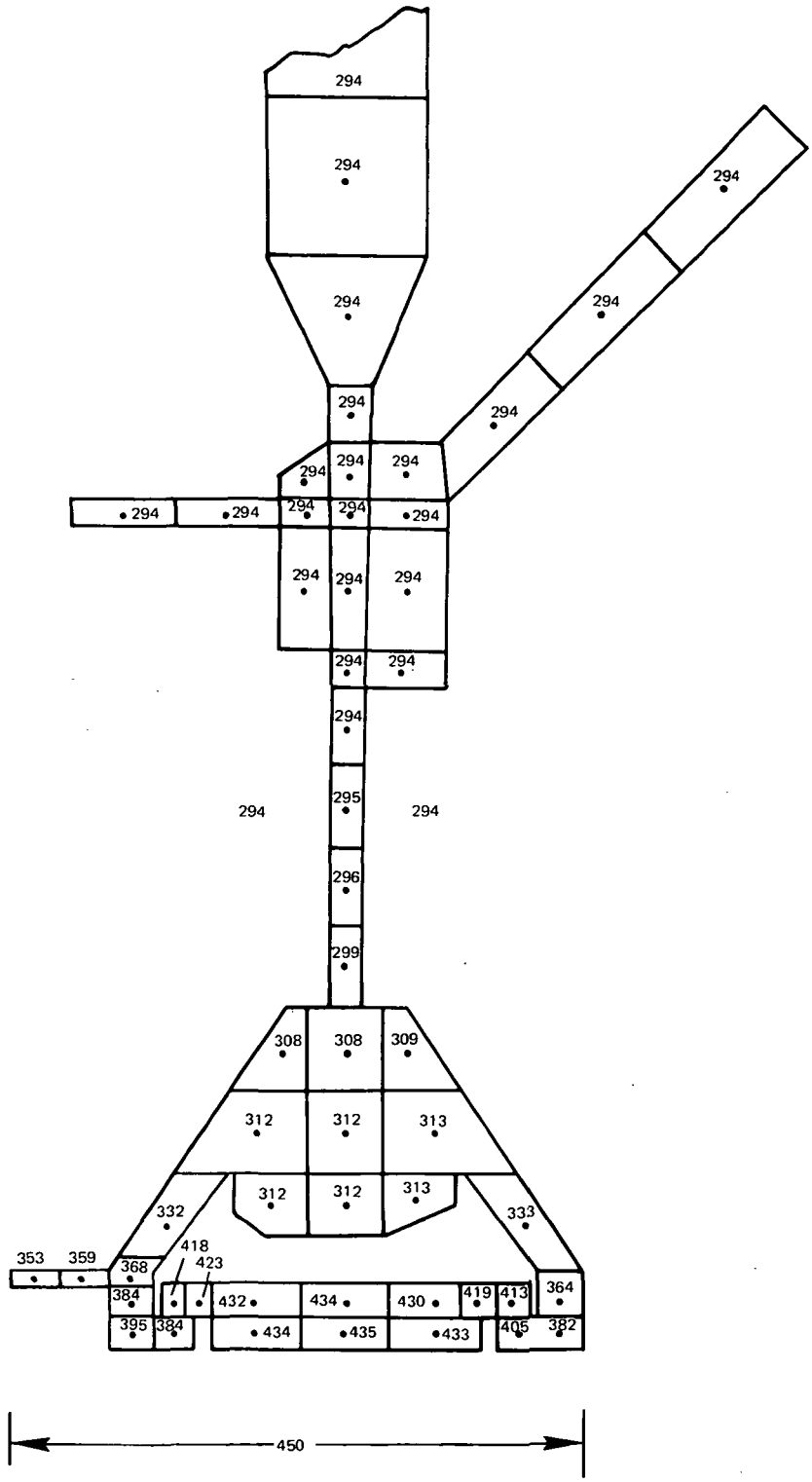

Figure 14 Rotor Temperature Distribution At Normal Operation Conditions - SI Units -°K

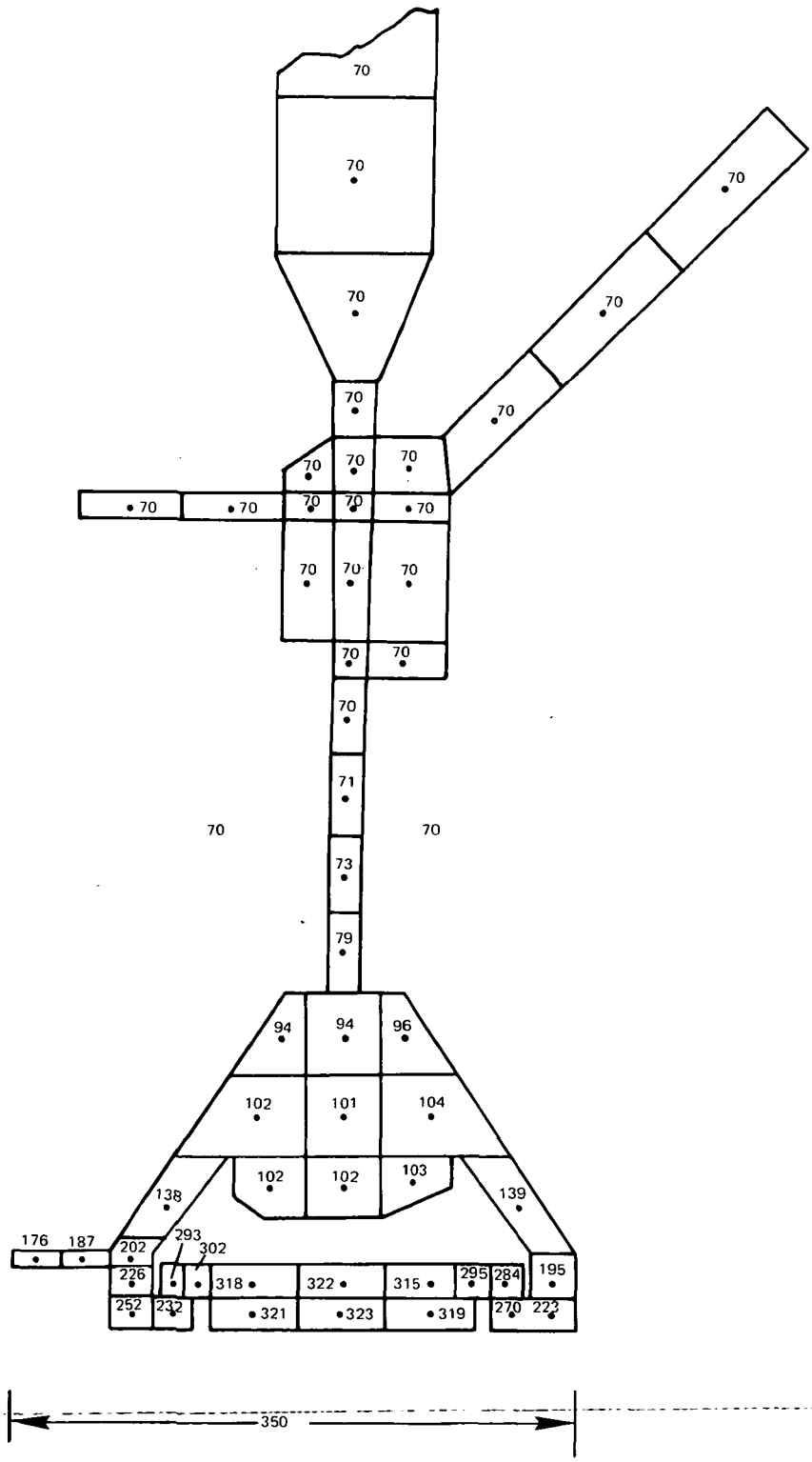

Figure 14A Rotor Temperature Distribution At Normal Operating Conditions - English Units ~ °F

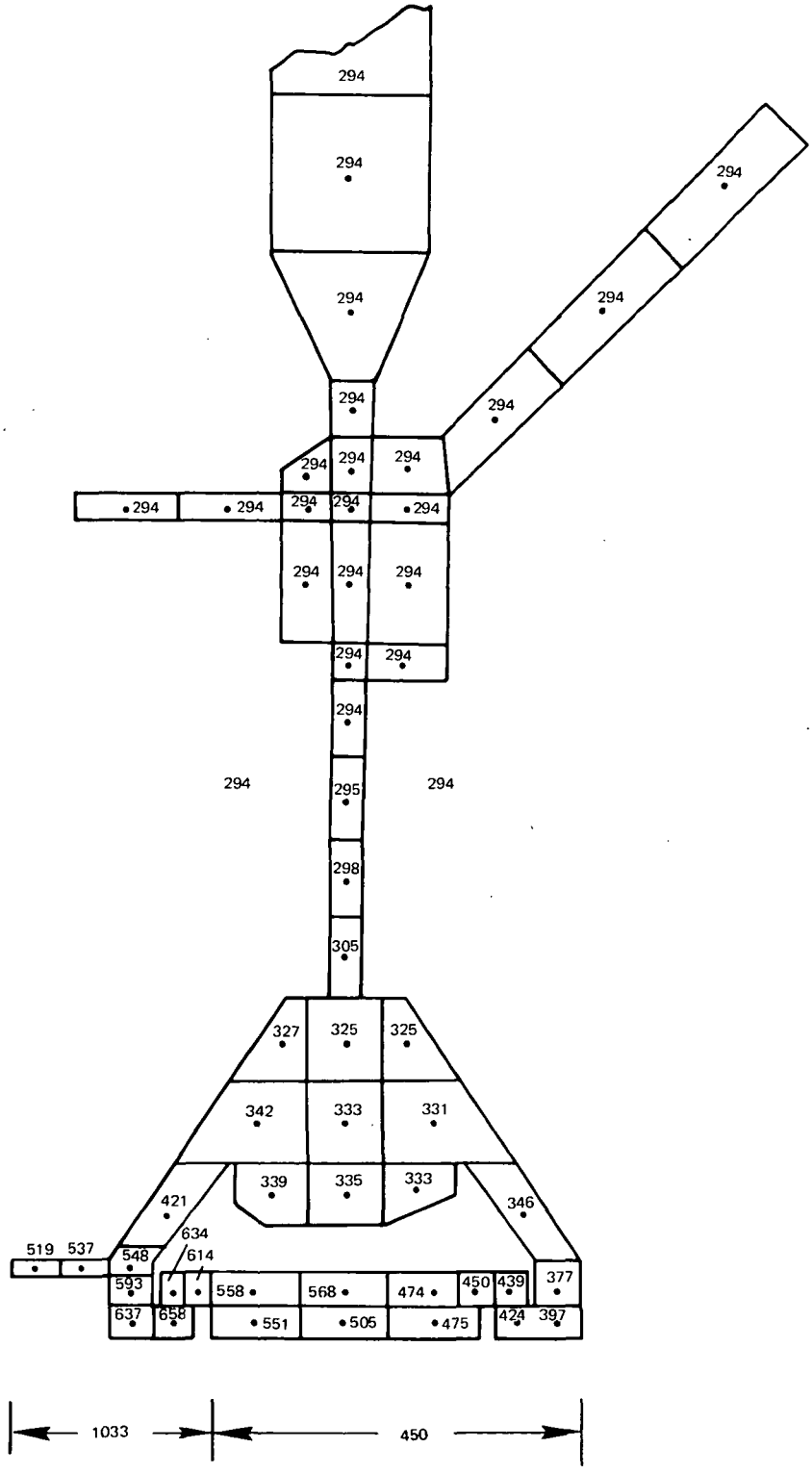

Figure 15 Rotor Temperature Distribution With No Buffer Gas Flow to Primary - SI Units ~ °K

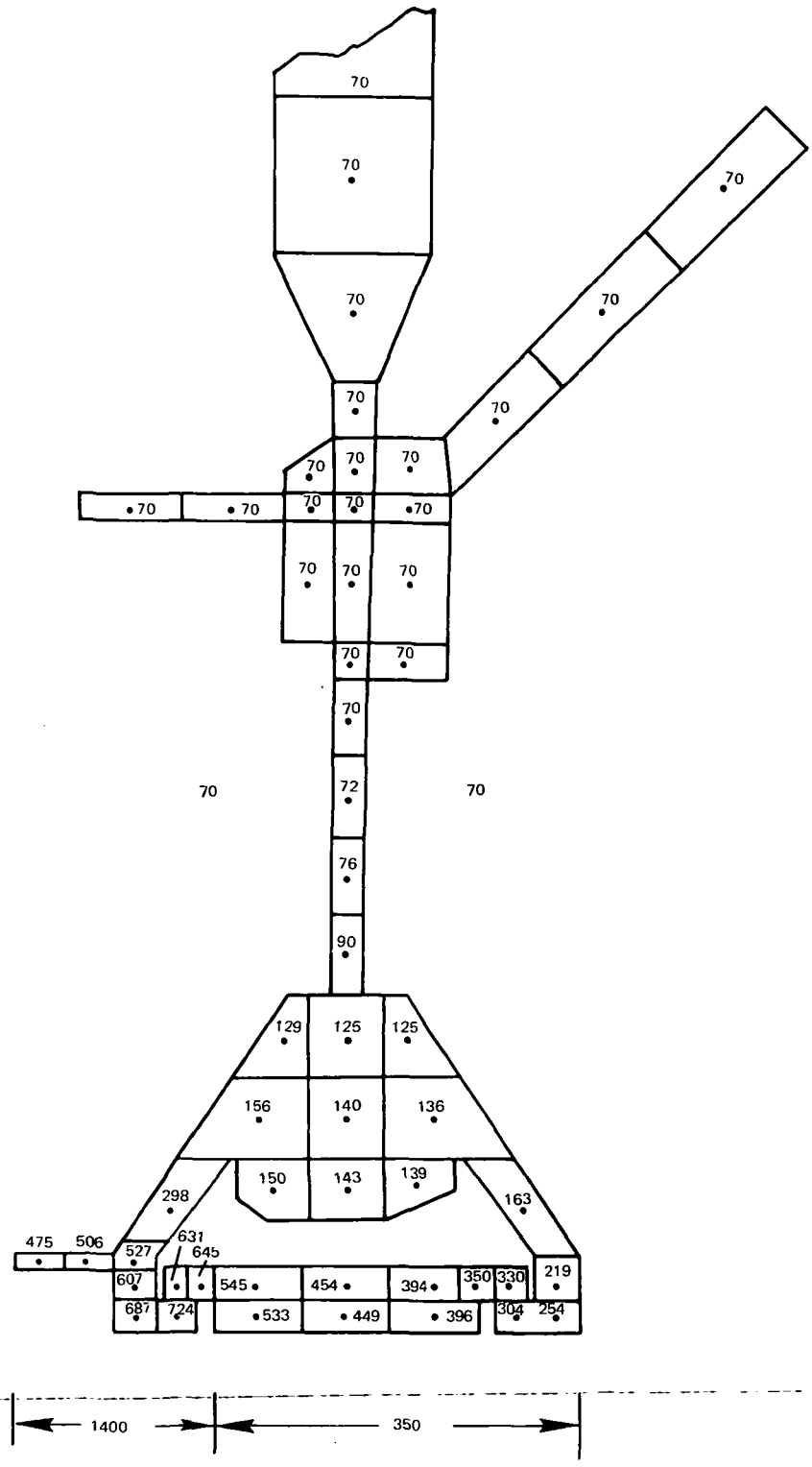

Figure 15A Rotor Temperature Distribution With No Buffer Gas Flow to Primary - English Units ~ °F

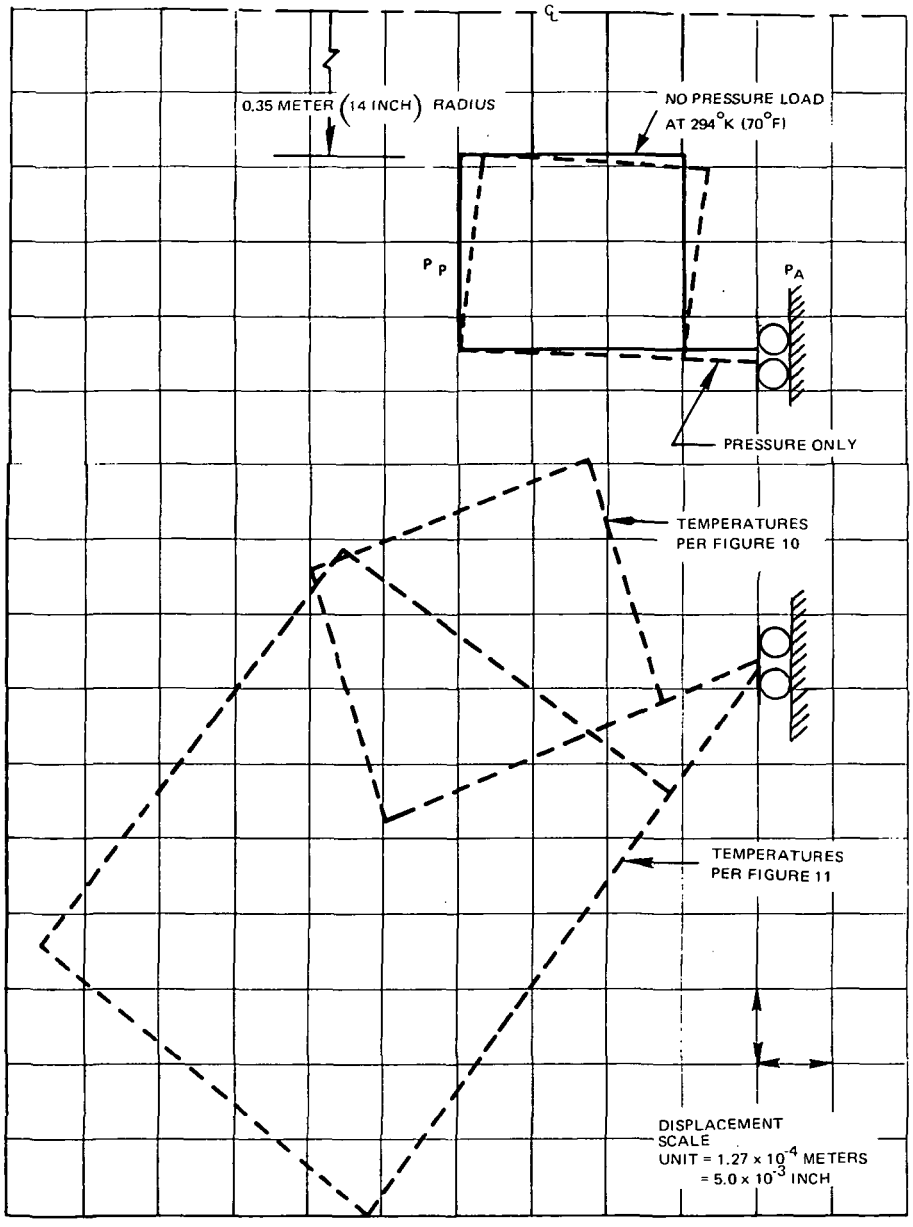

Figure 16 Effects of Axisymmetric Pressure Loading and Temperature Distribution on Seal Stator Structure

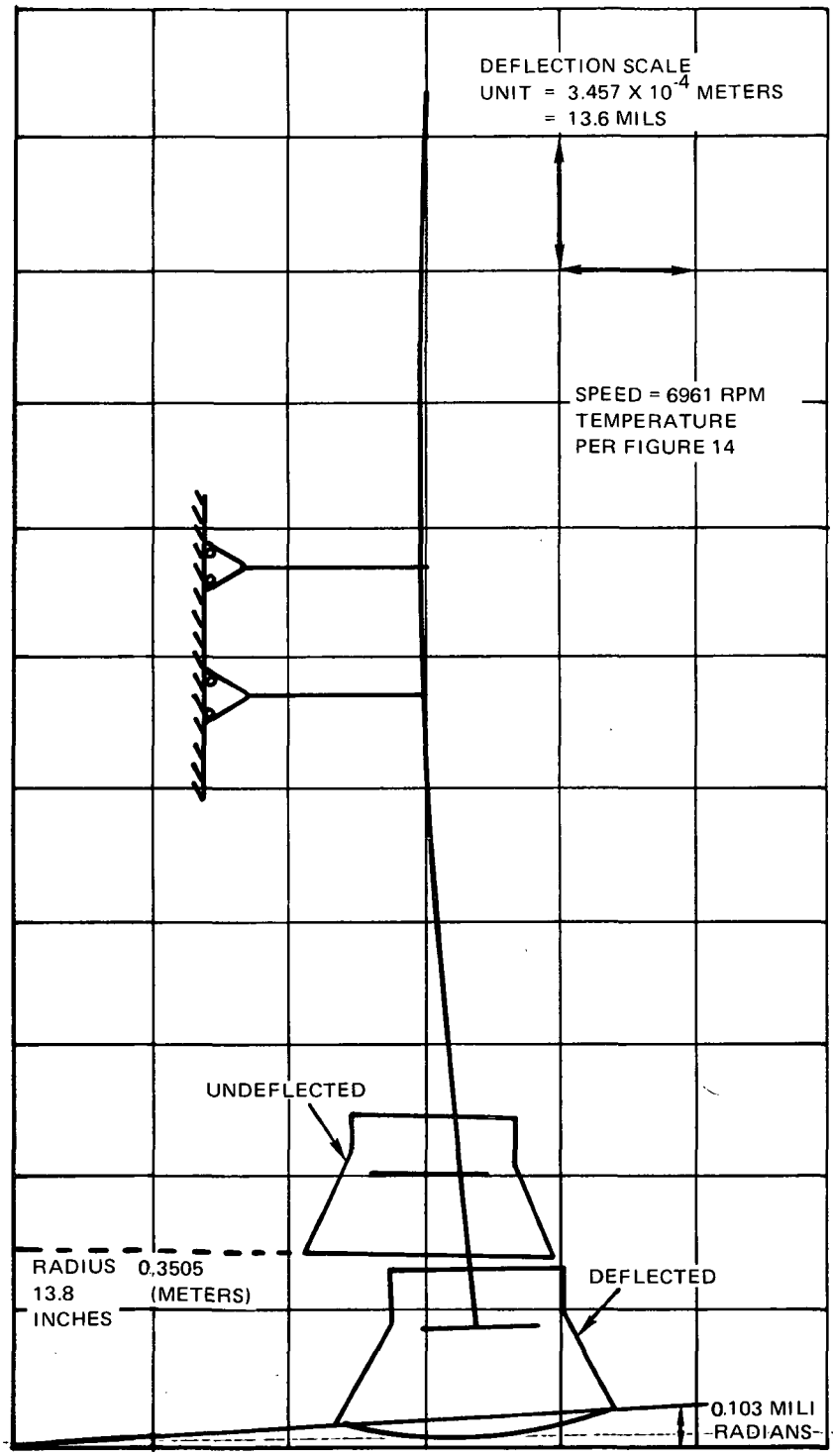

Figure 17 Effects of Pressure, Temperature and Speed on Rotor Structure at Normal Operating Conditions

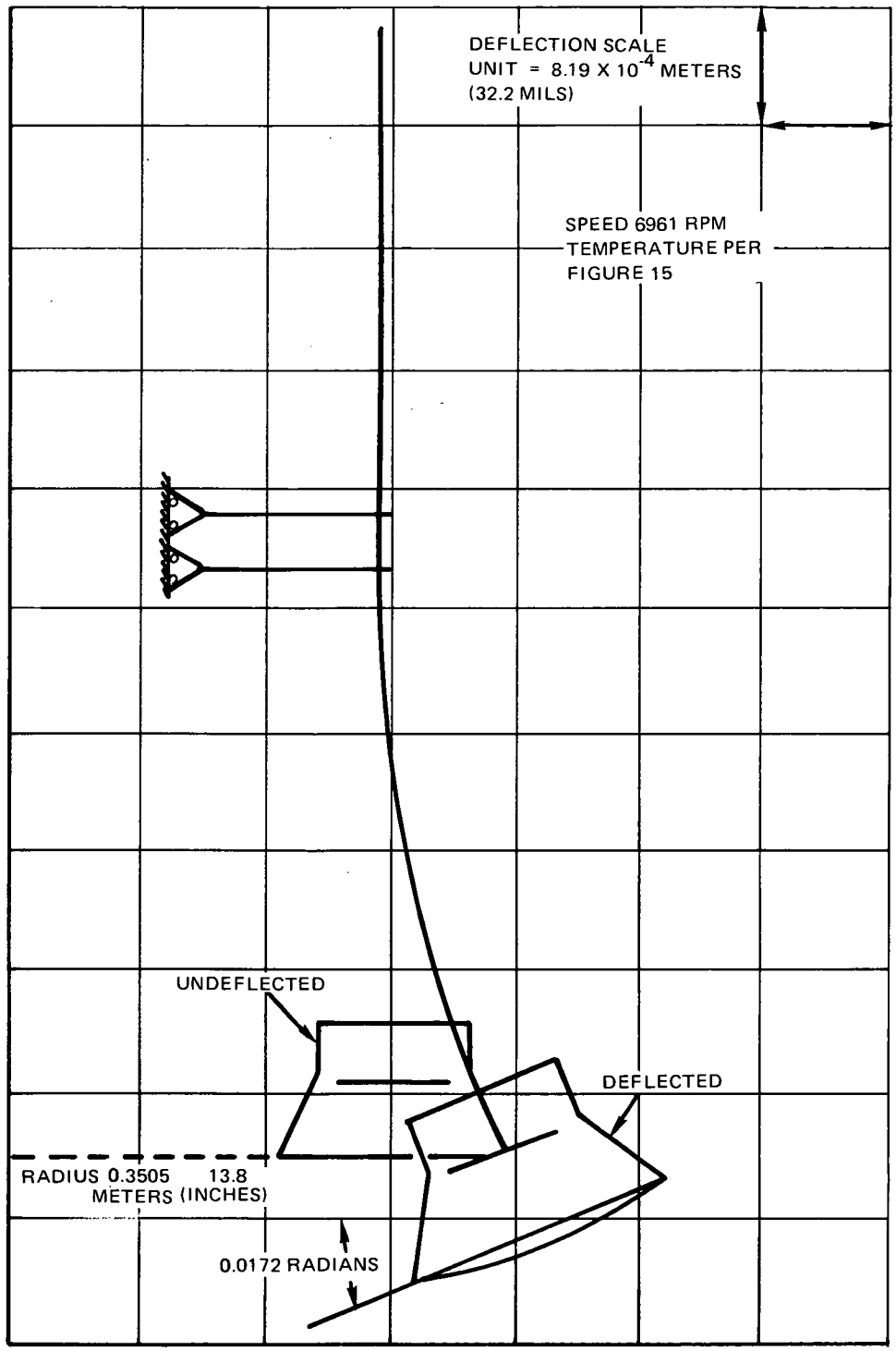

Figure 18 Effects of Pressure, Temperature and Speed on Rotor Structure With No Buffer Gas Flow to Primary

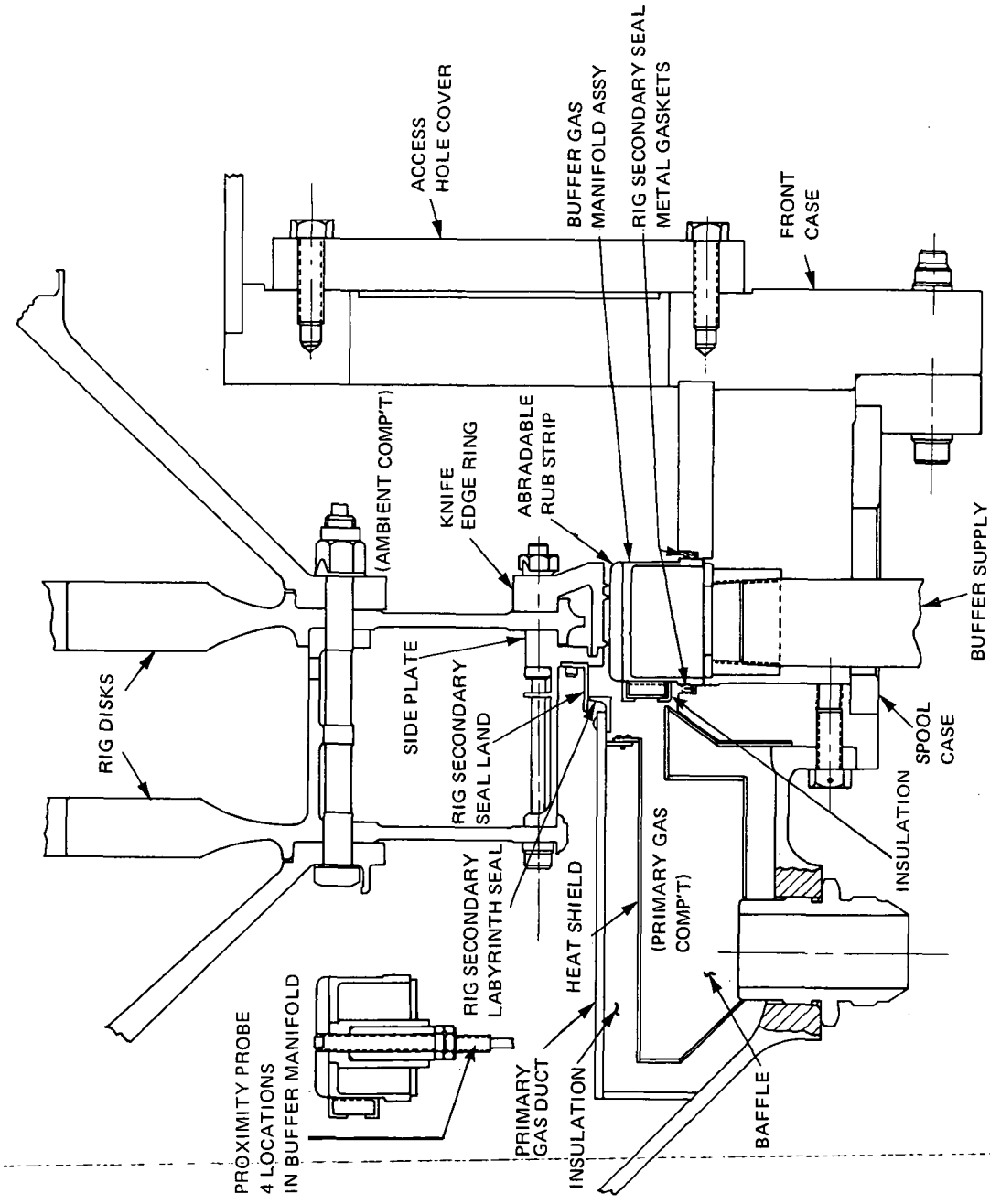

Figure 19 Test Seal and Rig Layout

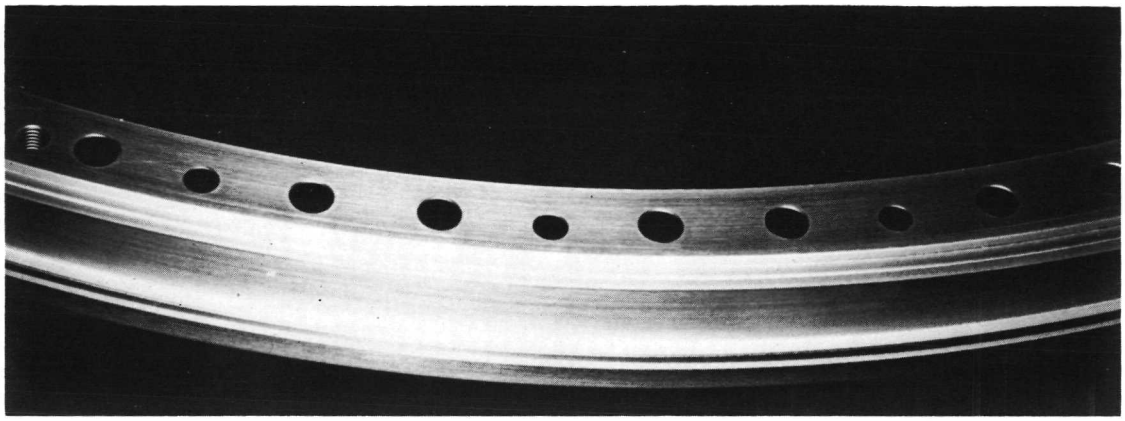

Figure 20 OD of Labyrinth Seal Ring Showing Knife Edge Seals

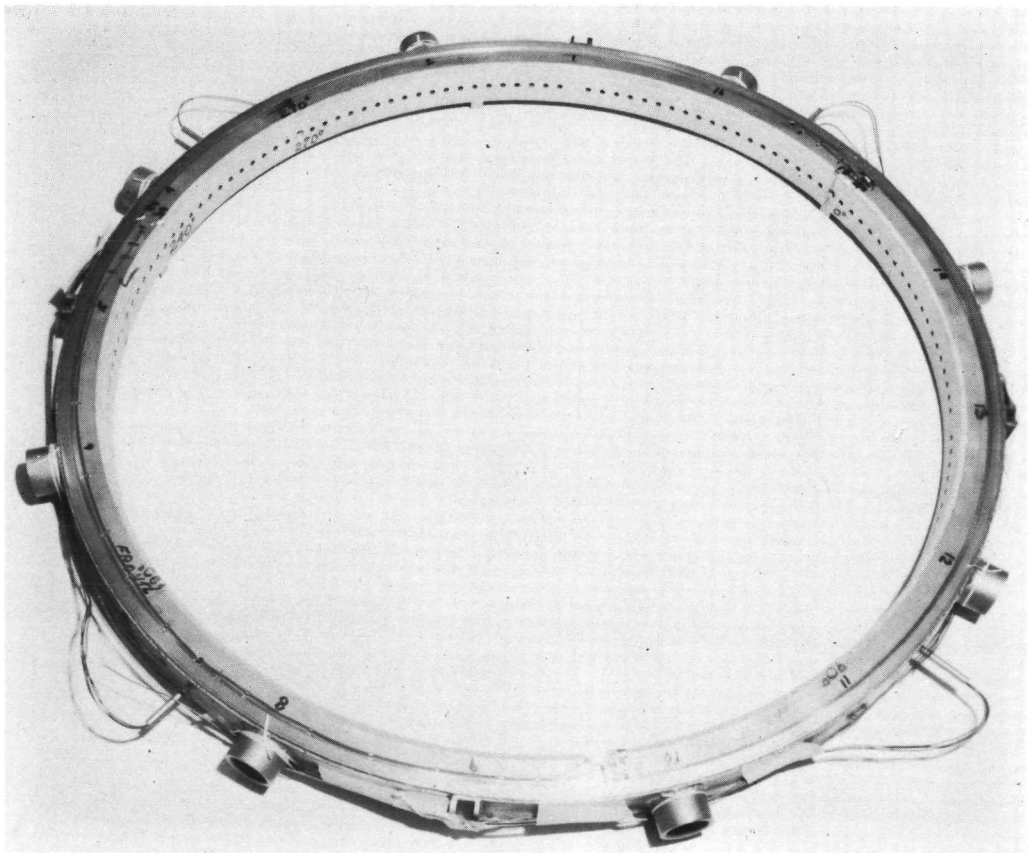

Figure 21 Seal Stator Assembly

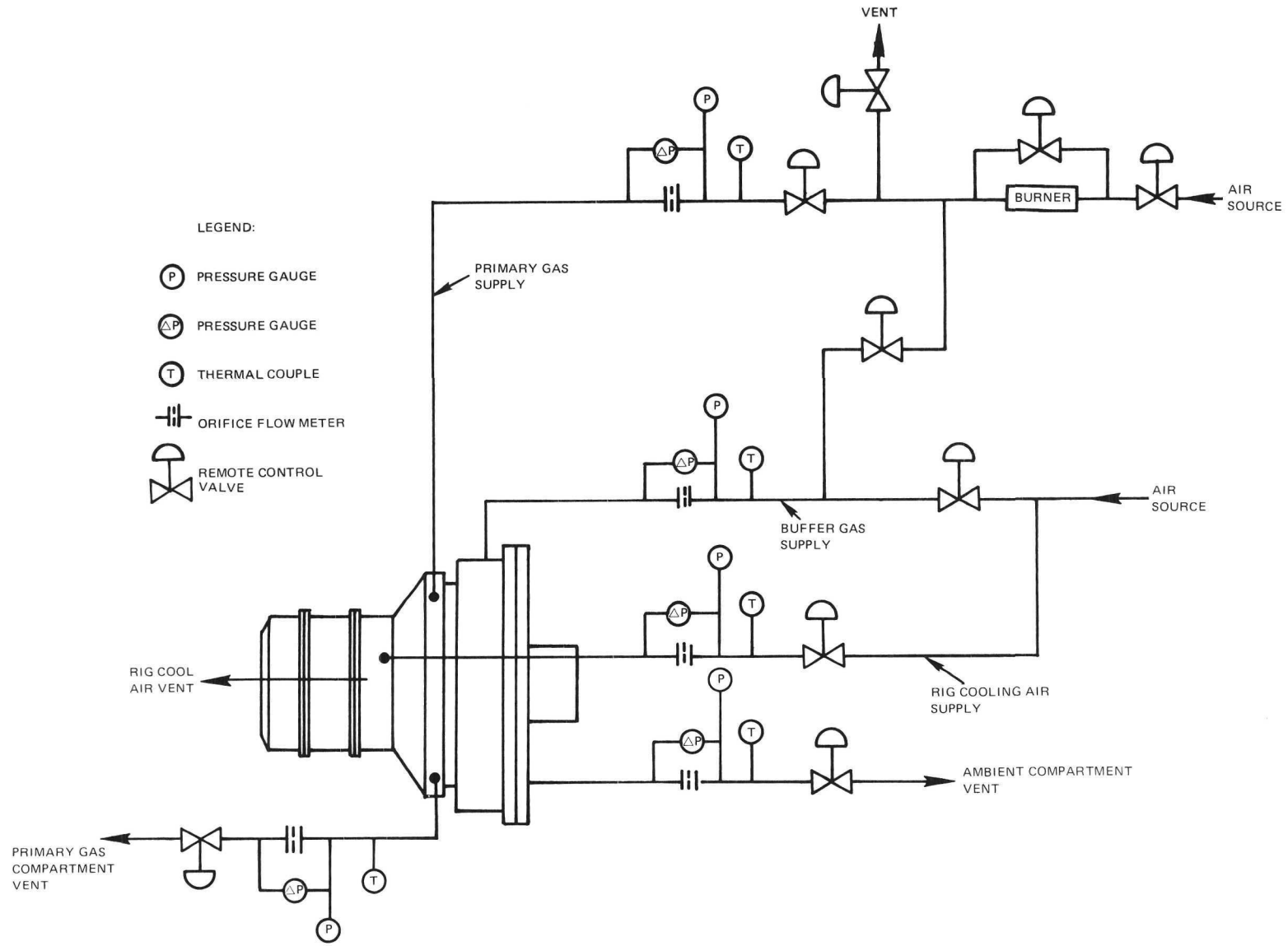

Figure 22 Air Flow System Schematic

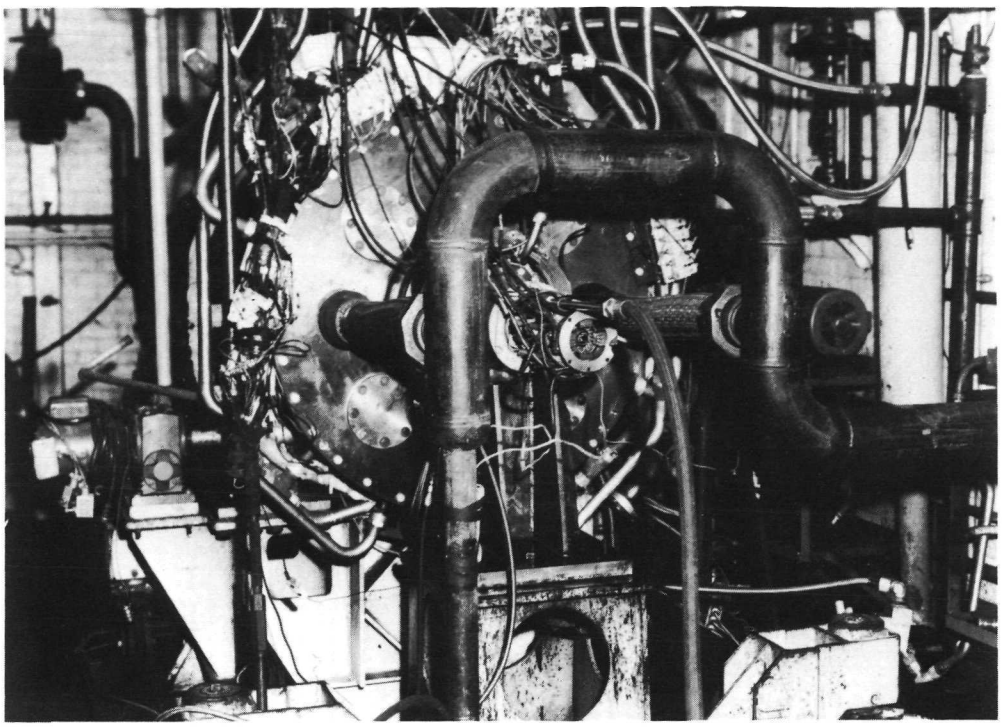

Figure 23 Rig Installed in Test Cell

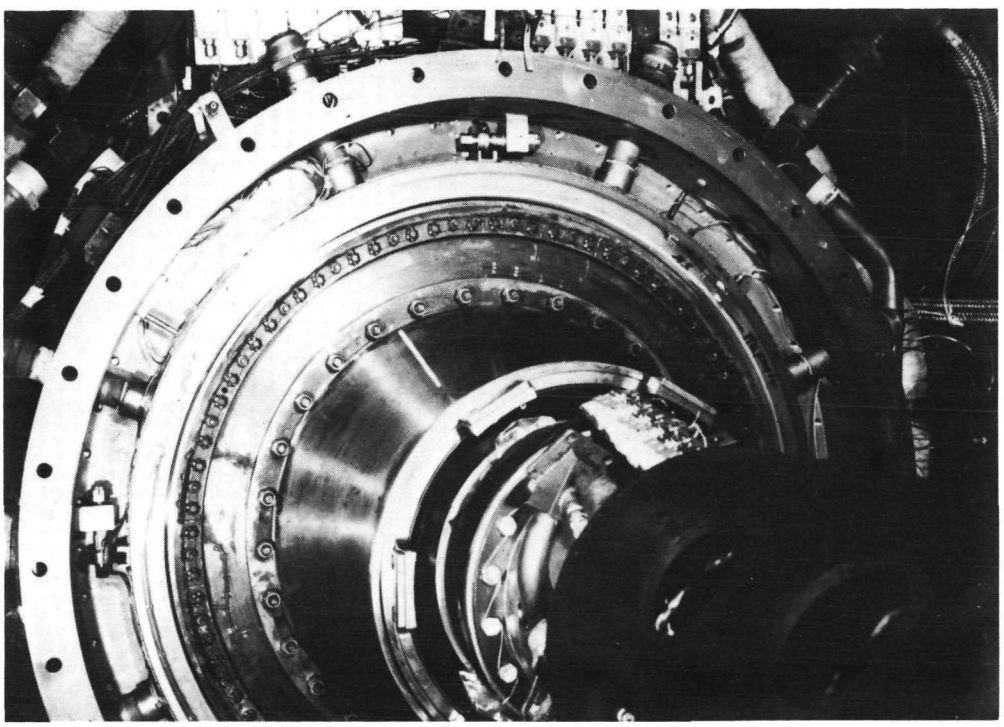

Figure 24 Test Seal Installed in Rig

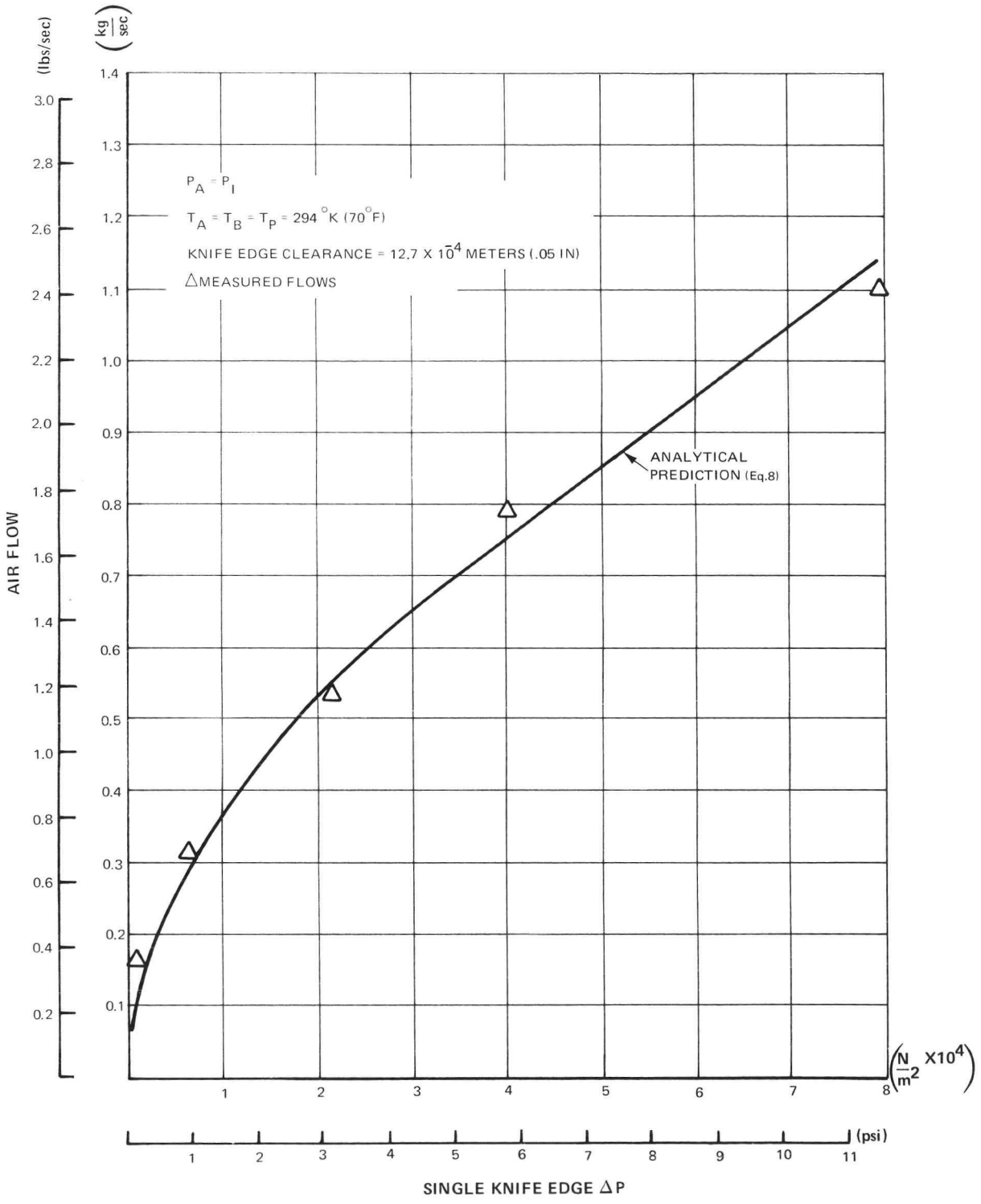

Figure 25 Build 1 - Static Calibration of Single Labyrinth at 12.7×10^{-4} Meters (.05 in.) Cold Clearance

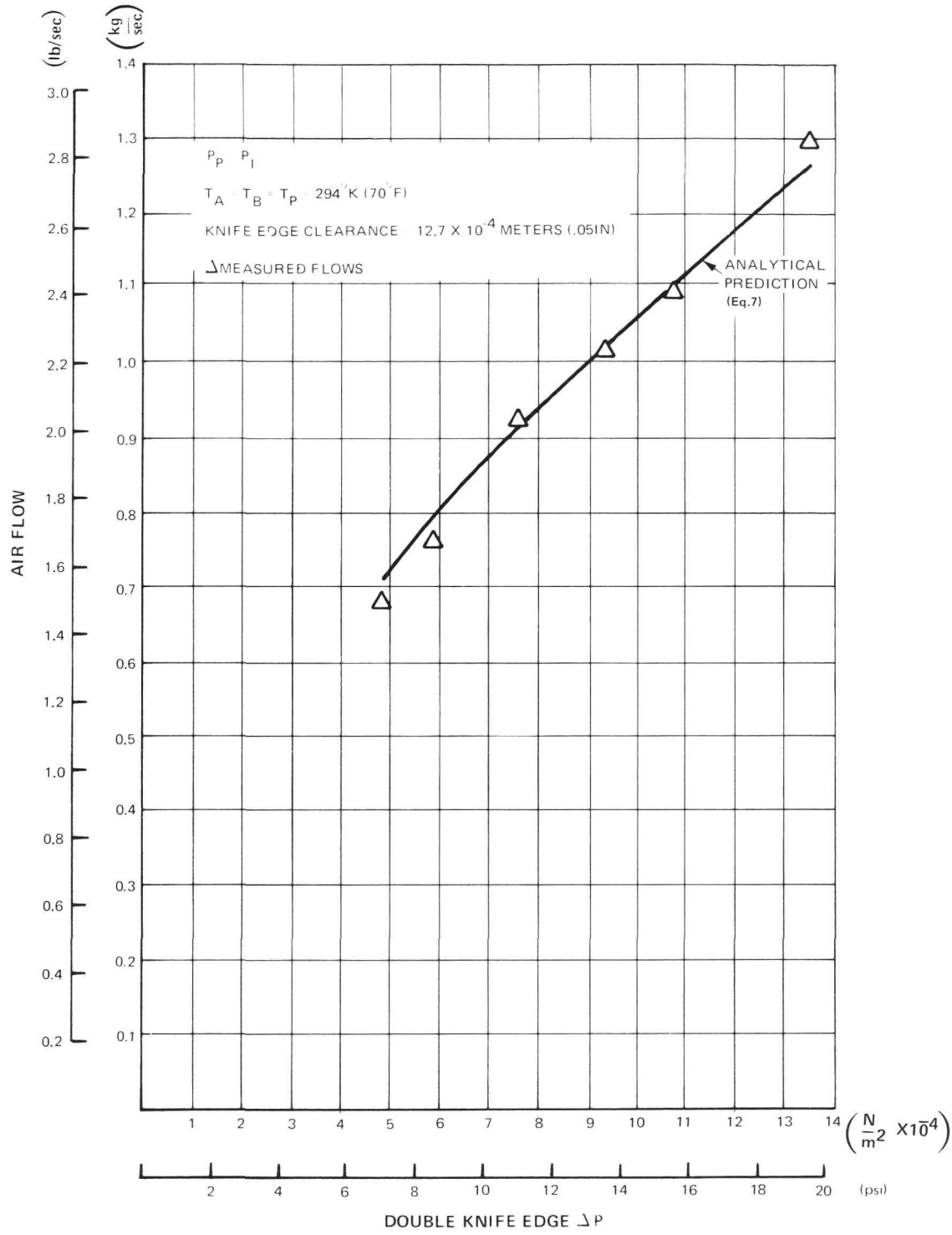

Figure 26 Build 1 - Static Calibration of Double Labyrinth at 12.7 x 10^{-4} Meters (.05 in.) Cold Clearance

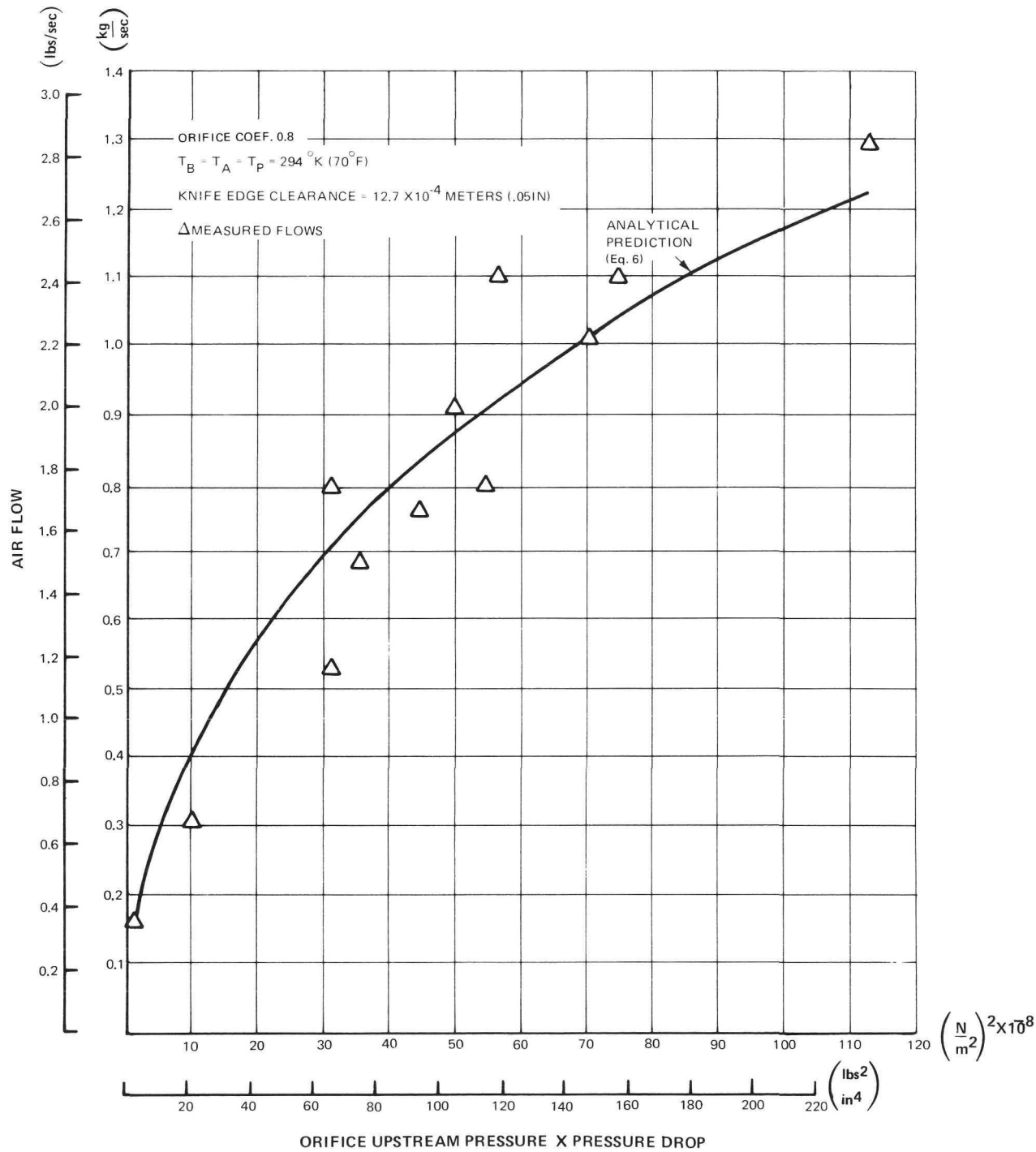

Figure 27 Build 1 - Buffer Gas Manifold Orifice Flow Calibration at 12.7×10^{-4} Meters (.05 in.) Cold Clearance

Figure 28 Buffer Gas Manifold Showing Flow Pattern

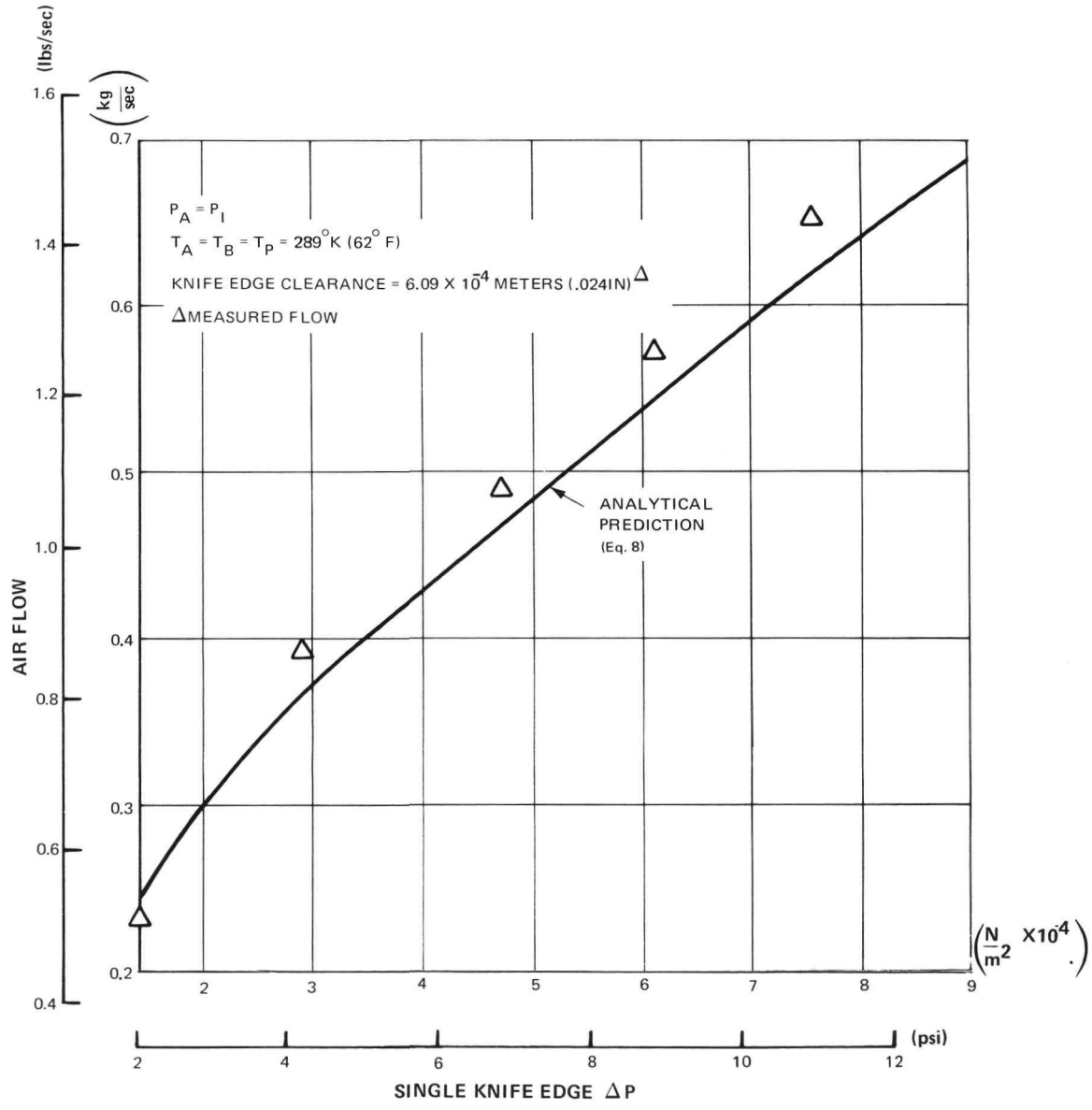

Figure 29 Build 2 - Static Calibration of Single Labyrinth at 6.09×10^{-4} Meters (.024 in.) Cold Clearance

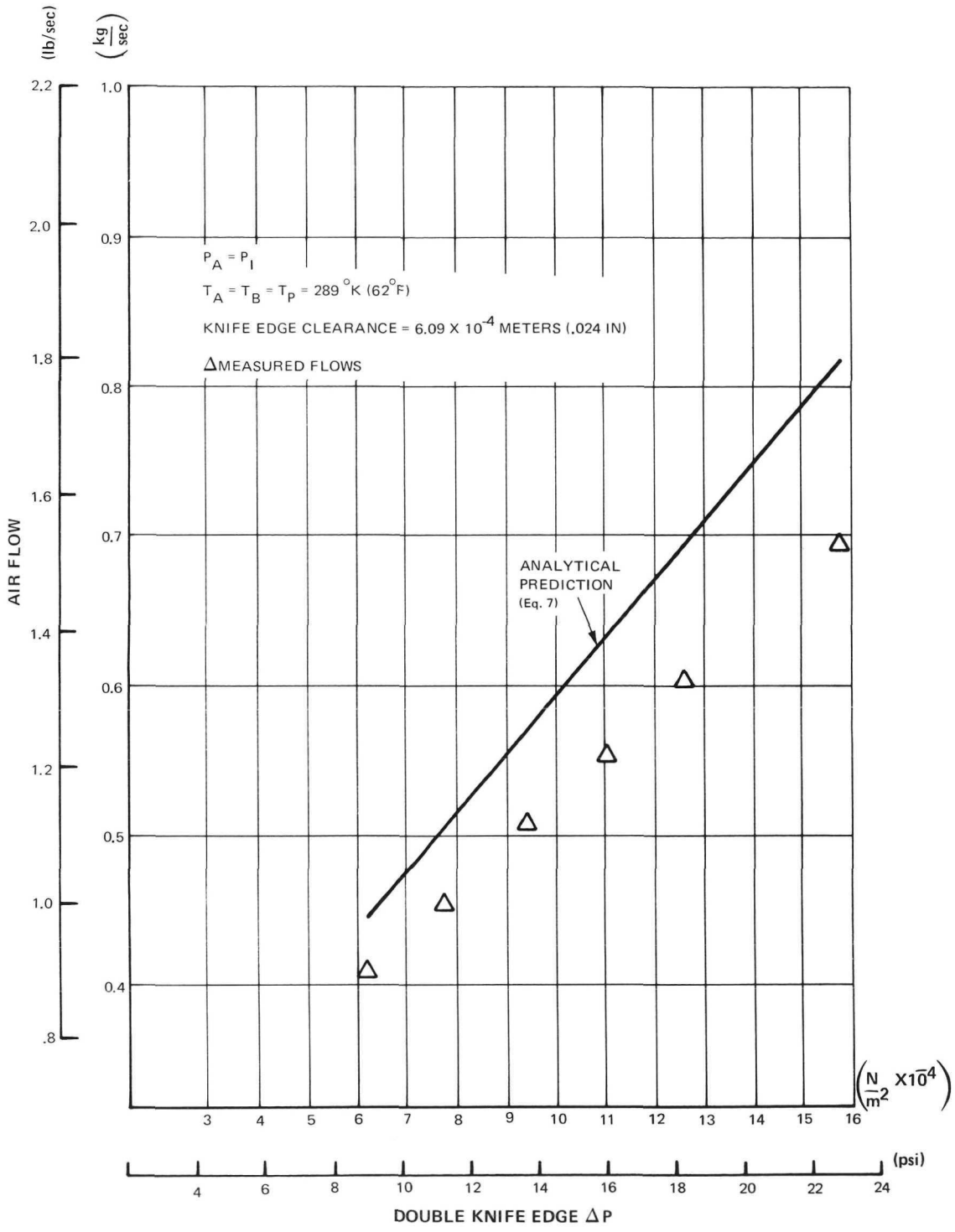

Figure 30 Build 2 - Static Calibration of Double Labyrinth at 6.09×10^{-4} Meters (.024 in.) Cold Clearance

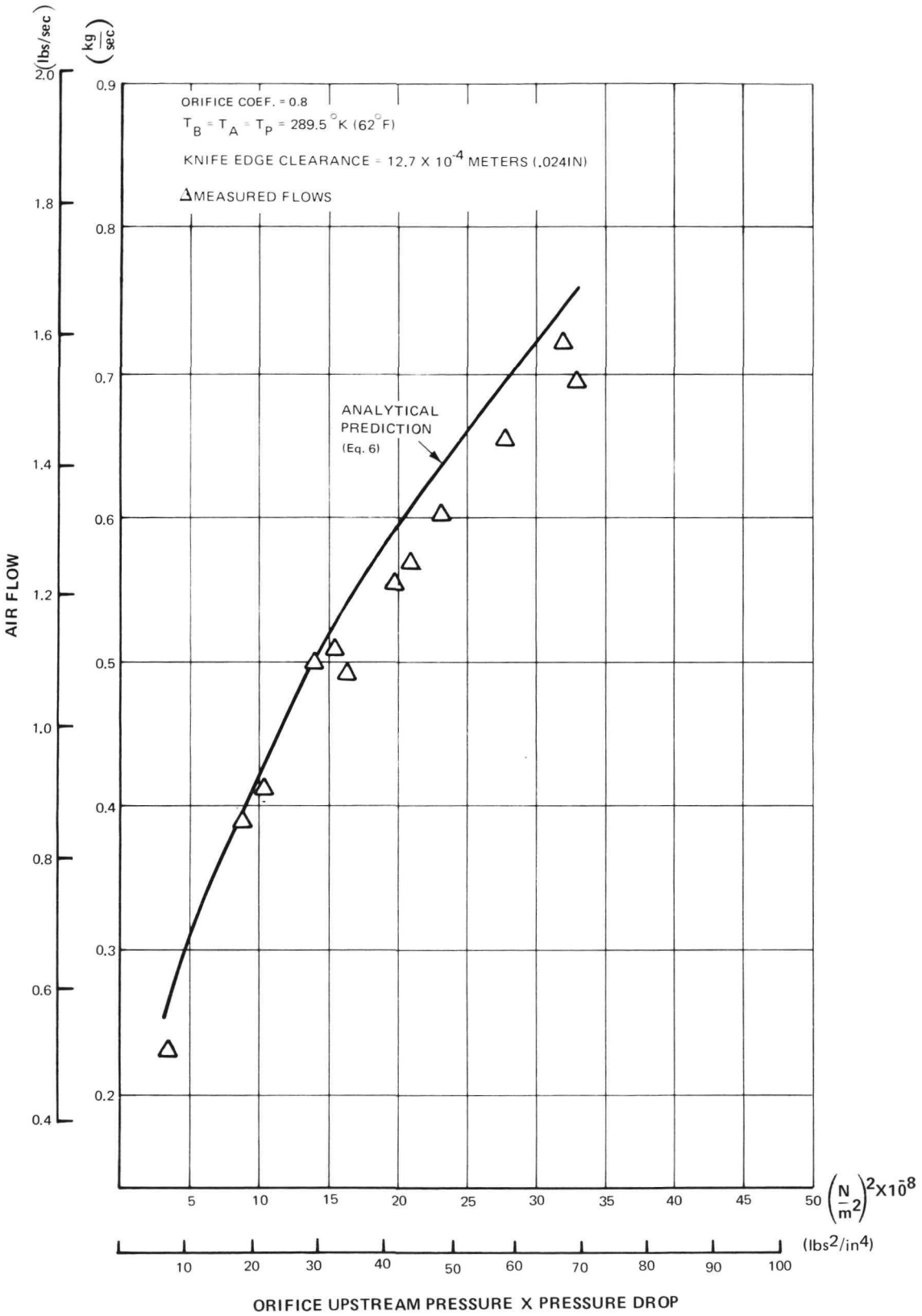

Figure 31 Build 2 - Buffer Gas Manifold Orifice Flow Calibration at 6.09×10^{-4} Meters Cold Clearance

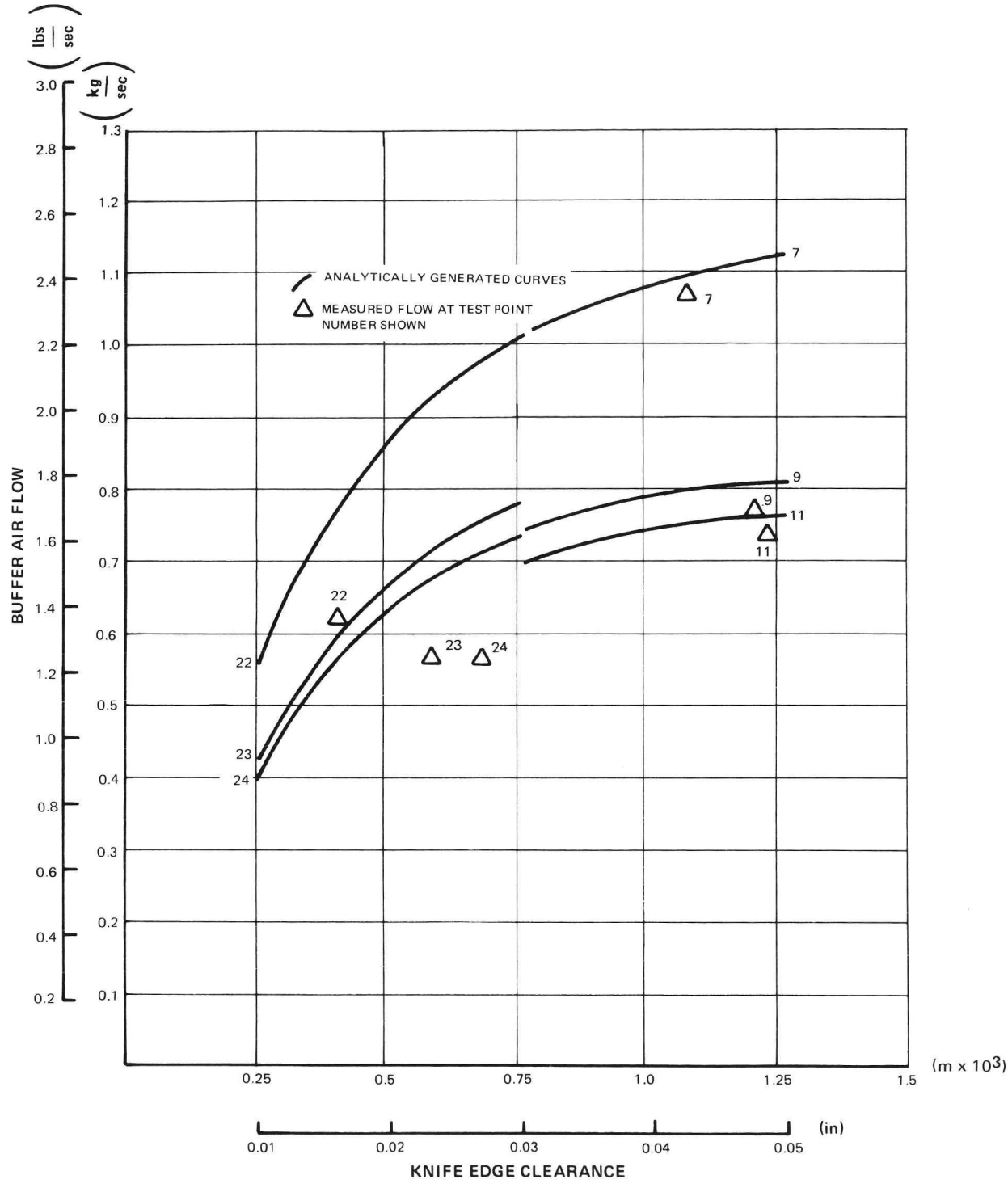

Figure 32 Measured Buffer Air Flow at Selected Dynamic Test Points Compared to Analytically Generated Curves at Test Point Gas Conditions

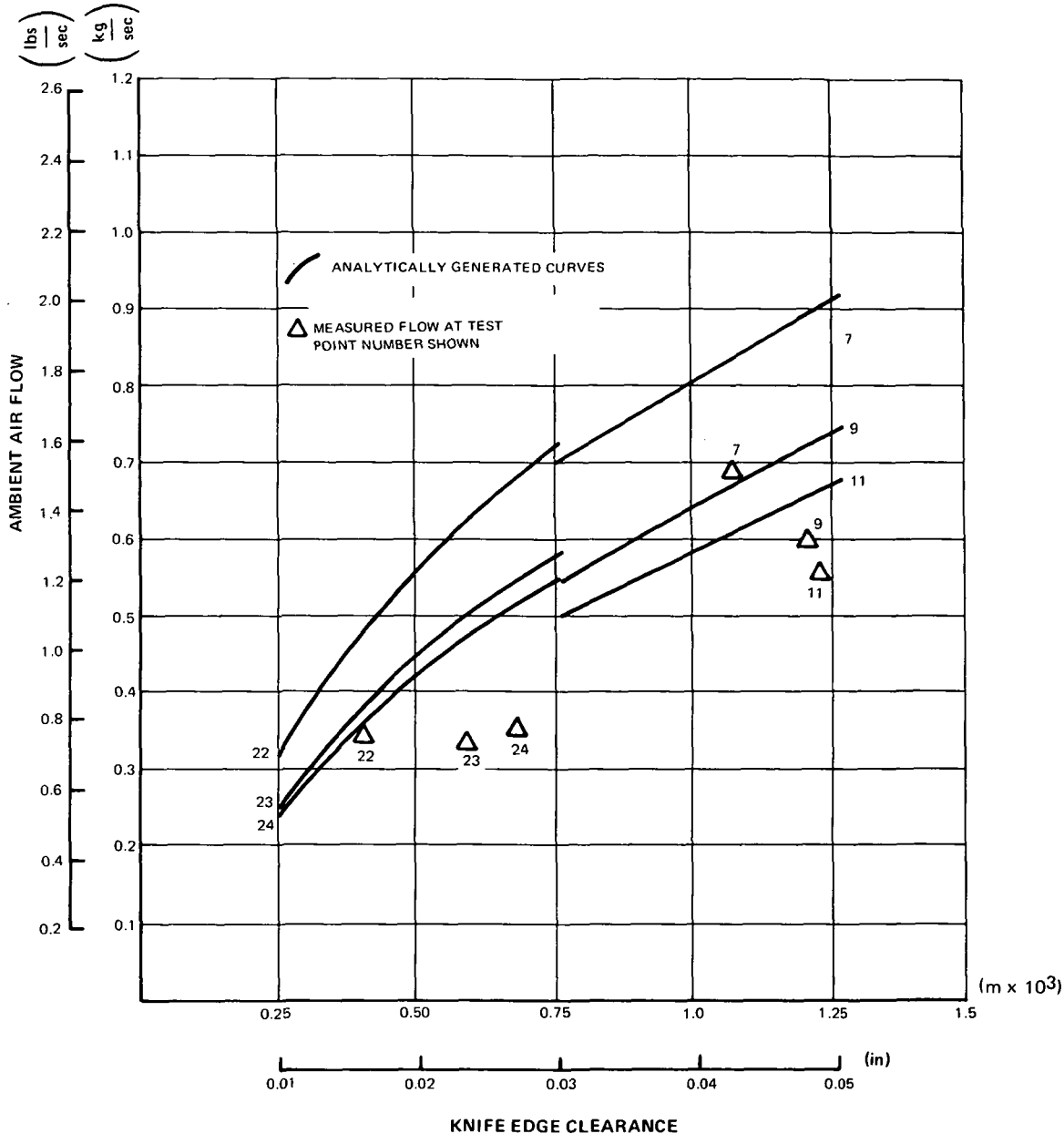

Figure 33 Measured Ambient Air Flow at Selected Dynamic Test Points Compared to Analytically Generated Curves at Test Point Gas Conditions

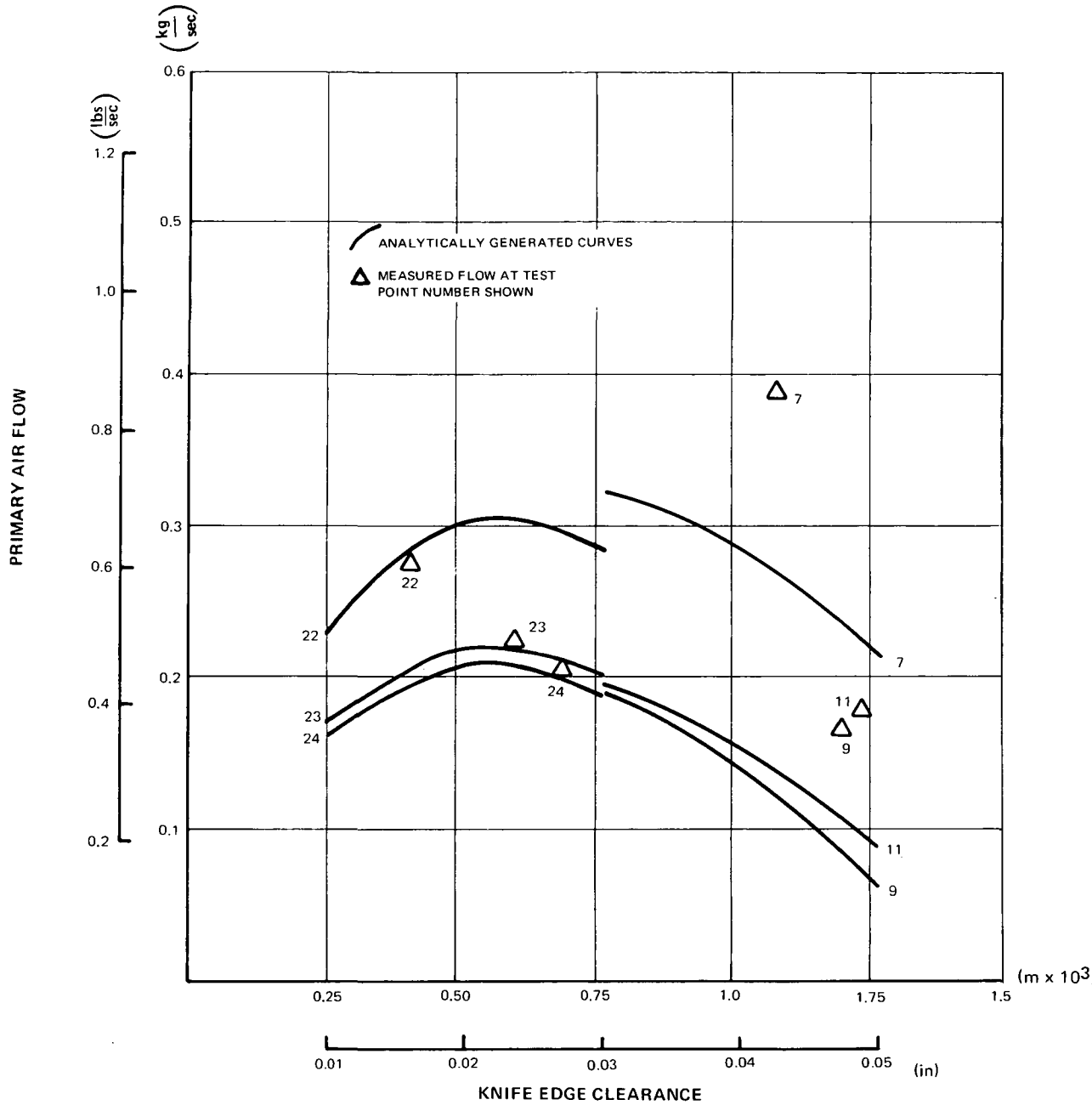

Figure 34 Measured Primary Air Flow at Selected Dynamic Test Points Compared to Analytically Generated Curves at Test Point Gas Conditions

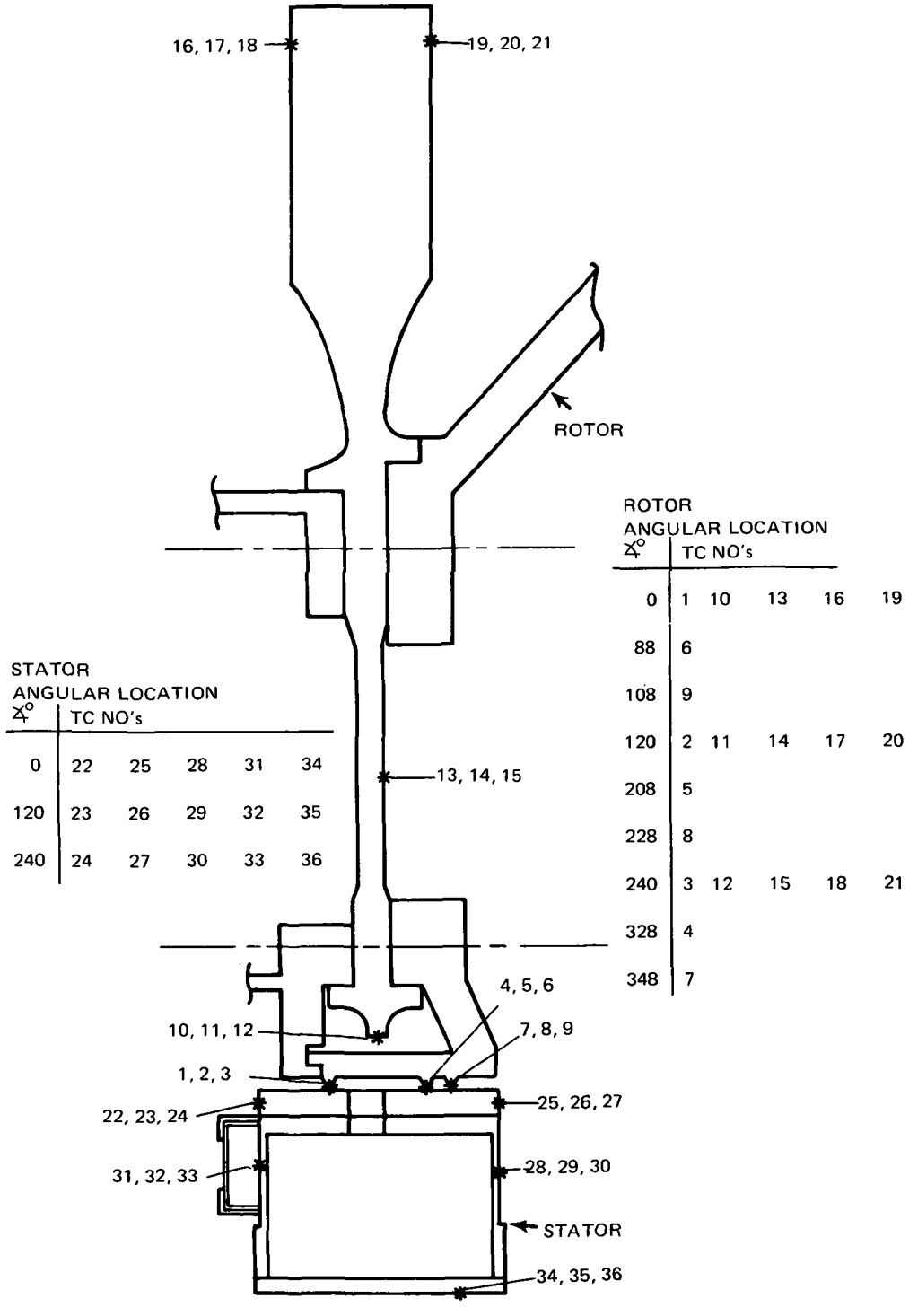

Figure 35 Rotor and Stator Thermocouple Locations.

Page Intentionally Left Blank

APPENDIX I

TABLES

TABLE I PREDICTED SEAL PERFORMANCE

Case	Pressure: Buffer	Primary	Ambient	Temperature: Buffer	Primary	Ambient	Rotor Speed	Radial Growth: Rotor	Stator	Operating Clearance Min.	Max.	Flow: W_1	W_2	W_3
	$N/m^2 \times 10^{-3}$ (psia)			°K (°F)			RPM	Meters $\times 10^3$ (Inch)		Meters $\times 10^3$	(Inch)	Kg/sec (lbs/sec)		
A	200.7 (30)	174 (25)	101.4 (14.7)	294 (70)	294 (70)	294 (70)	0	0	0	.063 1.27	(.025) (.050)	.871 (1.92) 1.002 (2.21)	.624 (1.375) .957 (2.11)	.247 (.545) .045 (.10)
B	200.7 (30)	174 (25)	101.4 (14.7)	294 (70)	294 (70)	294 (70)	6961	.330 (.013)	0	.304 .939	(.012) (.037)	.581 (1.280) .971 (2.14)	.356 (.785) .794 (1.75)	.225 (.495) .177 (.39)
C	200.7 (30)	174 (25)	101.4 (14.7)	394 (250)	922 (1200)	294 (70)	6961	.381 (.015)	.660 (.026)	.914 1.549	(.036) (.061)	.835 (1.84) Exceeds Max Clearance	.674 (1.485)	.161 (.355)
D	200.7 (30)	174 (25)	101.4 (14.7)	450 (350)	922 (1200)	294 (70)	6961	.406 (.016)	.863 (.034)	1.092 1.727	(.043) (.068)	.801 (1.765) Exceeds Max Clearance	.703 (1.55)	.098 (.215)
E	200.7 (30)	174 (25)	101.4 (14.7)	450 (350)	922 (1200)	294 (70)	6961	.736 (.029)	.863 (.034)	.762 1.397	(.030) (.055)	.746 (1.645) Exceeds Max Clearance	.562 (1.24)	.184 (.405)
F	200.7 (30)	174 (25)	101.4 (14.7)	294 (70)	294 (70)	294 (70)	0	0	0	.635 1.270	(.025) (.050)	1.710 (2.58) 1.374 (3.03)	.721 (1.59) 1.018 (2.245)	.449 (.99) .356 (.785)
G	200.7 (30)	174 (25)	101.4 (14.7)	294 (70)	294 (70)	294 (70)	6961	.330 (.013)	0	.304 .939	(.012) (.037)	.771 (1.70) 1.311 (2.89)	.426 (.94) .882 (1.945)	.345 (.76) .429 (.945)

TABLE II – BUILD 1 DYNAMIC TEST RESULTS

Test Point	Test Conditions								Measured Flows				Calculated Flows		
	Rig Speed-RPM	Static Seal Gap (Avg) Meters x 10^3 (Inch)	Buffer Gas Press N/m^2 x 10^{-3} (psia)	Buffer Gas Temp °K (°F)	Primary Gas Press N/m^2 x 10^{-3} (psia)	Primary Gas Temp °K (°F)	Ambient Comp't Press N/m^2 x 10^{-3} (psia)	Ambient Comp't Temp °K (°F)	W_1 Buffer Supply Kg/sec (lbs/sec)	W_2 Ambient Comp't Kg/sec (lbs/sec)	W_3 Primary Gas Comp't Kg/sec (lbs/sec)	Measured Seal Gap (Avg) Meters x 10^3 (Inch)	Buffer Supply Kg/sec (lbs/sec)	Ambient Comp't Kg/sec (lbs/sec)	Primary Comp't Kg/sec (lbs/sec)
7	3480	1.2 (49.8)	221.3 (32.1)	302 (84)	175.1 (24.4)	304 (88)	115.6 (16.76)	305 (90)	1.08 (2.38)	0.68 (1.51)	0.40 (0.87)	1.27 (.0426)	1.11 (2.44)	0.84 (1.85)	0.27 (0.59)
8	3480	1.2 (49.8)	236.5 (34.3)	303 (85)	182.7 (26.5)	305 (90)	118.2 (17.15)	306 (92)	1.13 (2.49)	0.74 (1.63)	0.39 (0.86)	1.08 (.0426)	1.22 (2.68)	0.90 (1.98)	0.32 (0.70)
9	3480	1.2 (49.8)	200.6 (29.1)	394 (250)	170.3 (24.7)	369 (205)	114.9 (16.66)	389 (242)	0.77 (1.70)	0.60 (1.33)	0.17 (0.37)	1.20 (.0474)	0.81 (1.78)	0.72 (1.59)	0.09 (0.19)
10	3480	1.2 (49.8)	236.5 (34.3)	391 (245)	182.0 (26.4)	386 (235)	116.9 (16.96)	390 (243)	0.96 (2.12)	0.62 (1.36)	0.34 (0.76)	1.05 (.0412)	1.06 (2.34)	0.78 (1.72)	0.29 (0.63)
11	3480	1.2 (49.8)	201.3 (29.2)	462 (371)	168.2 (24.4)	415 (287)	115.2 (16.71)	450 (352)	0.73 (1.62)	0.55 (1.23)	0.18 (0.39)	1.23 (.0486)	0.77 (1.69)	0.67 (1.47)	0.10 (0.22)
12	3480	1.2 (49.8)	238.6 (34.6)	461 (370)	180.6 (26.2)	444 (340)	116.6 (16.91)	453 (357)	0.91 (2.00)	0.58 (1.27)	0.33 (0.73)	1.08 (.0424)	1.00 (2.22)	0.73 (1.61)	0.27 (0.61)
13	3480	1.2 (49.8)	119.3 (28.9)	308 (95)	180.0 (26.4)	926 (1208)	115.2 (16.71)	322 (120)	0.70 (1.54)	0.73 (1.61)	-0.03 (-0.07)	1.06 (.0418)	W_2 Exceeds W_1		
14	3480	1.2 (49.8)	214.4 (31.1)	385 (233)	194.4 (28.2)	940 (1233)	118.2 (17.15)	399 (260)	0.73 (1.61)	0.69 (1.52)	0.04 (0.09)	1.21 (.0475)	W_2 Exceeds W_1		
15	0	1.2 (49.8)	219.9 (31.9)	300 (80)	168.9 (24.5)	300 (80)	116.2 (16.86)	299 (80)	1.07 (2.35)	0.73 (1.62)	0.33 (0.73)	1.27 (.0498)	1.16 (2.55)	0.88 (1.93)	0.28 (0.62)

TABLE III – BUILD 2 DYNAMIC TEST RESULTS

Test Point	Test Conditions: Rig Speed-RPM	Static Seal Gap (Avg) Meters x 10^3 (Inch)	Buffer Gas Press N/m^2 x 10^{-3} (psi)	Buffer Gas Temp °K (°F)	Primary Gas Press N/m^2 x 10^{-3} (psi)	Primary Gas Temp °K (°F)	Ambient Comp't Press N/m^2 x 10^{-3} (psi)	Ambient Comp't Temp °K (°F)	Measured Flows: W_1 Buffer Supply Kg/sec (lbs/sec)	W_2 Ambient Comp't Kg/sec (lbs/sec)	W_3 Primary Gas Comp't Kg/sec (lbs/sec)	Measured Seal Gap (Avg) Meters x 10^3 (inch)	Calculated Flows: Buffer Supply Kg/sec (lbs/sec)	Ambient Comp't Kg/sec (lbs/sec)	Primary Comp't Kg/sec (lbs/sec)
22	3480	0.6 (.024)	216.4 (31.39)	291 (64)	174.8 (25.35)	292 (66)	105.1 (15.24)	302 (84)	.62 (1.37)	.35 (.77)	.27 (.60)	.41 (.016)	.77 (1.70)	.48 (1.06)	.29 (.64)
23	3480	0.6 (.024)	204.3 (29.68)	397 (255)	170.8 (24.77)	387 (236)	106.8 (15.49)	391 (244)	.57 (1.25)	.34 (.74)	.23 (.51)	.59 (.0233)	.72 (1.59)	.50 (1.11)	.22 (.48)
24	3480	0.6 (.024)	208.4 (30.17)	461 (370)	173.5 (25.16)	443 (337)	107.8 (14.63)	444 (340)	.57 (1.26)	.36 (.79)	.21 (.47)	.68 (.0269)	.72 (1.58)	.52 (1.14)	.20 (.44)
25	5030	0.6 (.024)	241.2 (34.98)	478 (400)	186.0 (26.98)	871 (1108)	104.7 (15.19)	473 (392)	.48 (1.05)	.25 (.55)	.23 (.50)	.56 (.022)	.84 (1.85)	.54 (1.19)	.30 (.66)
26	5950	0.6 (.024)	261.4 (37.92)	465 (377)	194.8 (28.25)	967 (1280)	103.7 (15.04)	509 (456)	.25 (.56)	.15 (.32)	.11 (.24)	.12 (.0048)	.29 (.64)	.15 (.34)	.14 (.30)
27	5950	0.6 (.024)	246.9 (35.81)	454 (357)	188.7 (27.37)	960 (1268)	103.1 (14.95)	528 (490)	.15 (.33)	0 (0)	.15 (.33)	.13 (.0051)	.29 (.63)	.15 (.34)	.13 (.29)
28	5950	0.6 (.024)	222.6 (32.28)	390 (242)	179.9 (26.09)	967 (1280)	103.1 (14.95)	504 (447)	.13 (.29)	0 (0)	.13 (.29)	0 (0)	0 (0)	0 (0)	0 (0)
29	5950	0.6 (.024)	257.1 (37.29)	394 (250)	187.7 (27.22)	963 (1273)	103.1 (14.95)	487 (416)	.21 (.46)	0 (0)	.21 (.46)	.43 (.017)	.0127 (.028)	.00635 (.014)	.00635 (.014)
30	0	0.6 (.024)	219.9 (31.89)	290 (62)	172.4 (25.01)	291 (64)	108.5 (15.73)	289 (61)	.83 (1.82)	.49 (1.07)	.34 (.75)	.54 (.0214)	.94 (2.07)	.60 (1.32)	.34 (.75)

Apparent Seal Rub

TABLE IV

DYNAMIC TEST – ROTOR AND SEAL STATOR TEMPERATURES

T/C # Per Fig. 35	TEST POINT 7 °K (°F)	8 °K (°F)	9 °K (°F)	10 °K (°F)	11 °K (°F)	12 °K (°F)	13 °K (°F)	14 °K (°F)
1	304 (88)	304 (88)	385 (233)	392 (246)	445 (342)	458 (364)	331 (137)	400 (260)
2	304 (88)	304 (88)	385 (233)	392 (246)	445 (342)	458 (365)	333 (139)	401 (263)
3	304 (88)	304 (88)	385 (234)	392 (246)	446 (343)	458 (365)	333 (139)	402 (264)
4	303 (86)	303 (85)	389 (240)	390 (243)	444 (339)	455 (360)	319 (115)	390 (243)
5	303 (86)	303 (85)	389 (240)	390 (243)	443 (338)	455 (360)	319 (115)	390 (242)
6	296 (73)	296 (73)	384 (231)	375 (216)	437 (327)	450 (350)	314 (105)	380 (225)
7	300 (80)	300 (81)	338 (148)	332 (138)	351 (173)	354 (177)	311 (100)	339 (150)
8	301 (82)	303 (86)	389 (240)	391 (245)	443 (338)	455 (360)	320 (116)	390 (242)
9	301 (82)	303 (86)	389 (240)	393 (248)	444 (339)	455 (360)	320 (117)	390 (242)
10	311 (100)	311 (100)	373 (211)	396 (253)	435 (324)	454 (358)	331 (137)	380 (224)
11	311 (100)	311 (100)	374 (213)	396 (253)	435 (324)	454 (358)	331 (137)	380 (225)
12	311 (100)	311 (100)	355 (180)	375 (216)	401 (262)	415 (287)	329 (132)	362 (192)
13	313 (104)	313 (103)	368 (203)	394 (250)	430 (314)	448 (347)	328 (130)	374 (213)
14	313 (104)	313 (103)	371 (208)	394 (250)	431 (316)	449 (349)	327 (129)	375 (216)
15	313 (104)	313 (103)	371 (208)	394 (250)	431 (316)	449 (349)	327 (129)	375 (216)
16	320 (117)	321 (118)	324 (123)	375 (216)	355 (179)	394 (250)	320 (116)	329 (132)
17	320 (117)	321 (118)	323 (121)	375 (216)	354 (178)	394 (249)	319 (115)	328 (130)
18	320 (117)	321 (118)	323 (121)	375 (216)	354 (178)	394 (249)	319 (115)	328 (130)
19	320 (117)	321 (118)	323 (122)	375 (215)	355 (180)	394 (249)	319 (115)	328 (130)
20	308 (95)	316 (109)	324 (124)	375 (215)	355 (180)	394 (249)	319 (115)	328 (130
21	320 (116)	321 (118)	324 (124)	375 (215)	355 (180)	394 (249)	319 (115)	328 (130)
22	305 (90)	305 (90)	386 (236)	393 (248)	444 (340)	459 (367)	404 (268)	519 (475)
23	304 (88)	305 (90)	389 (240)	390 (242)	450 (351)	454 (358)	344 (159)	434 (330)
24	304 (88)	305 (90)	390 (242)	390 (242)	452 (354)	455 (360)	349 (168)	423 (482)
25	301 (83)	303 (85)	391 (245)	390 (242)	455 (360)	455 (360)	323 (121)	394 (250)
26	301 (82)	303 (85)	389 (241)	388 (238)	453 (355)	451 (353)	312 (102)	373 (212)
27	301 (82)	301 (83)	390 (242)	388 (238)	455 (359)	454 (358)	310 (99)	379 (222)
28	305 (89)	305 (90)	393 (248)	391 (245)	455 (360)	456 (362)	317 (111)	384 (232)
29	304 (88)	305 (89)	390 (243)	389 (241)	450 (350)	454 (358)	312 (102)	376 (218)
30	304 (87)	304 (88)	393 (248)	390 (242)	456 (362)	456 (361)	313 (103)	382 (228)
31	305 (90)	300 (80)	361 (190)	361 (190)	405 (269)	405 (270)	343 (158)	397 (255)
32	303 (85)	303 (85)	389 (240)	388 (238)	451 (353)	397 (255)	371 (208)	444 (339)
33	303 (85)	303 (85)	390 (242)	388 (238)	451 (353)	399 (258)	328 (130)	440 (333)
34	304 (87)	303 (85)	393 (247)	388 (239)	454 (358)	399 (259)	323 (122)	393 (248)
35	303 (85)	303 (85)	390 (243)	388 (238)	451 (353)	398 (257)	323 (121)	385 (233)
36	302 (84)	303 (85)	390 (243)	388 (238)	450 (350)	399 (258)	318 (112)	386 (236)

TABLE IV (Cont'd)

DYNAMIC TEST – ROTOR AND SEAL STATOR TEMPERATURES

T/C # Per Fig. 35	TEST POINT 22 °K (°F)	23 °K (°F)	24 °K (°F)	25 °K (°F)	26 °K (°F)	27 °K (°F)	28 °K (°F)	29 °K (°F)
1	297 (75)	385 (234)	441 (335)	503 (445)	544 (520)	507 (453)	472 (390)	462 (372)
2	297 (75)	385 (234)	441 (335)	501 (442)	542 (515)	507 (453)	476 (397)	466 (379)
3	297 (75)	385 (234)	442 (336)	501 (442)	540 (513)	503 (445)	480 (405)	469 (385)
4	297 (75)	387 (237)	447 (345)	489 (420)	511 (460)	497 (435)	466 (380)	459 (367)
5	297 (75)	387 (237)	447 (345)	488 (419)	526 (487)	497 (435)	470 (386)	461 (370)
6	297 (75)	388 (239)	449 (348)	489 (420)	532 (498)	496 (434)	473 (391)	464 (375)
7	294 (70)	333 (139)	356 (182)	355 (179)	363 (193)	350 (170)	339 (150)	339 (150)
8	297 (75)	386 (236)	445 (342)	489 (420)	531 (496)	505 (449)	478 (400)	468 (382)
9	298 (76)	387 (237)	445 (342)	489 (420)	531 (497)	504 (447)	483 (410)	475 (395)
10	298 (76)	396 (254)	395 (251)	455 (360)	509 (457)	546 (523)	492 (426)	488 (418)
11	298 (76)	395 (252)	371 (209)	403 (266)	436 (325)	328 (130)	346 (163)	355 (180)
12	298 (76)	349 (168)	379 (222)	442 (336)	495 (431)	496 (433)	479 (402)	470 (387)
13	300 (81)	355 (180)	389 (240)	473 (392)	539 (510)	546 (523)	529 (492)	523 (482)
14	301 (82)	358 (184)	292 (246)	474 (393)	539 (510)	545 (522)	529 (492)	523 (481)
15	301 (82)	357 (183)	390 (243)	474 (394)	539 (510)	545 (522)	528 (492)	522 (480)
16	294 (70)	312 (102)	321 (118)	408 (275)	492 (426)	530 (495)	531 (497)	529 (492)
17	294 (70)	311 (101)	320 (116)	408 (275)	491 (425)	529 (493)	531 (497)	529 (492)
18	294 (70)	311 (101)	320 (116)	408 (275)	491 (425)	529 (493)	530 (495)	529 (493)
19	294 (70)	313 (103)	322 (120)	405 (270)	488 (419)	526 (488)	530 (495)	528 (490)
20	289 (60)	313 (103)	323 (122)	391 (245)	459 (367)	511 (460)	514 (465)	523 (482)
21	293 (67)	313 (103)	323 (122)	404 (267)	488 (418)	525 (485)	530 (494)	526 (487)
22	INOPERATIVE THERMOCOUPLE							
23	INOPERATIVE THERMOCOUPLE							
24	293 (68)	392 (246)	454 (357)	540 (512)	864 (1095)	865 (1098)	876 (1117)	721 (838)
25	295 (72)	389 (241)	450 (350)	471 (389)	500 (440)	497 (435)	467 (381)	460 (369)
26	293 (68)	389 (240)	446 (344)	494 (430)	529 (493)	513 (463)	456 (362)	450 (351)
27	294 (69)	390 (242)	448 (347)	467 (381)	509 (457)	506 (452)	465 (377)	456 (361)
28	295 (71)	389 (241)	447 (345)	469 (384)	495 (432)	496 (433)	466 (380)	459 (367)
29	295 (72)	389 (241)	444 (340)	485 (413)	515 (468)	502 (444)	467 (381)	455 (360)
30	295 (72)	390 (243)	444 (340)	468 (382)	493 (427)	494 (430)	454 (358)	450 (351)
31	INOPERATIVE THERMOCOUPLE							
32	292 (66)	388 (238)	440 (332)	607 (632)	632 (678)	586 (596)	517 (471)	505 (449)
33	282 (48)	390 (242)	444 (340)	523 (482)	628 (671)	632 (678)	604 (627)	589 (600)
34	INOPERATIVE THERMOCOUPLE							
35	292 (66)	389 (240)	442 (336)	498 (436)	509 (453)	483 (410)	428 (310)	426 (308)
36	291 (64)	390 (242)	445 (342)	466 (380)	493 (428)	491 (424)	453 (355)	450 (350)

APPENDIX II

LIST OF SYMBOLS

A – Leakage area ~ meters^2 (inch^2)

A_o – Buffer gas supply orifice area ~ meters^2 (inch^2)

K_f – Flow coefficient ~ dimensionless

N – Number of knife edges

N_o – Number of buffer gas supply orifices

P_A – Ambient gas pressure ~ N/m^2 (psia)

P_B – Buffer gas pressure – N/m^2 (psia)

P_I – Intermediate pressure ~ N/m^2 (psia)

P_P – Primary gas pressure ~ N/m^2 (psia)

P_d – Downstream pressure ~ N/m^2 (psia)

P_u – Upstream pressure ~ N/m^2 (psia)

T – Temperature ~ °K (°F)

T_A – Ambient gas temperature ~ °K (°F)

T_B – Buffer gas pressure ~ °K (°F)

T_P – Primary gas pressure ~ °K (°F)

W_1 – Buffer gas flow ~ kg/sec (lbs/sec)

W_2 – Ambient gas flow ~ kg/sec (lbs/sec)

W_3 – Primary gas flow ~ kg/sec (lbs/sec)

Y – Expansion factor ~ dimensionless

e – Knife edge clearance ~ meters (inch)

h – Heat transfer film coefficient ~ $\frac{\text{joules}}{\text{hr m}^2\,°\text{K}}$ $\left(\frac{\text{BTU}}{\text{hr m}^2\,°\text{K}}\right)$

LIST OF SYMBOLS (Cont'd)

k – Ratio of specific heats ~ dimensionless

s – Knife edge spacing ~ meters (inch)

t – Knife edge thickness ~ meters (inch)

ΔP – Pressure differential ~ N/m^2 (psia)

α – Flow coefficient, function of N, P_d/P_m

γ – Carryover factor, function of N, e/s.

ρ_B – Buffer gas density ~ kg/m^3 (lbs/ft^3)

ρ_u – Upstream gas density ~ kg/m^3 (lbs/ft^3)

ϕ – Flow function, function of t, e/t

DISTRIBUTION LIST

Addressee	Copies
NASA Headquarters Washington, D.C. 20546	
Attn: N. F. Rekos (RL)	1
A. J. Evans (RH)	1
J. Maltz (RMW)	1
NASA Lewis Research Center 21000 Brookpark Road Cleveland, OH 44135	
Attn: A. Ginsburg, MS 5-3	1
E. E. Bisson, MS 5-3	1
C. H. Voit, MS 5-3	1
B. Lubarsky, MS 3-3	1
R. L. Johnson, MS 23-2	1
L. P. Ludwig, MS 23-2	1
T. N. Strom, MS 23-2	20
Contract Section A, MS 500-206	1
Report Control Office, MS 5-5	1
Library, MS 60-3	1
Technology Utilization Office, MS 3-19	1
NASA Scientific & Technical Information Facility P. O. Box 33 College Park, MD 20740	
Attn: NASA Representative	2
NASA Langley Research Center Langley Station Hampton, Va 23365	
Attn: Mark R. Nichols	1
Wright-Patterson Air Force Base Dayton, OH 45433	
Attn: AFAPL (APFL), J. L. Morris	1
SEJDF, S. Prete	1
AFML/XR, R. L. Adamczak	1
MANE, R. Headrick	1
MANL, L. M. Peterson	1
FAA Headquarters 800 Independence Ave., SW Washington, D. C. 20553	
Attn: F. B. Howard	1

Addressee	Copies
U.S. Naval Air Development Center Aeronautical Materials Dept. Warminster, PA 18974 Attn: A. L. Lockwood	1
U.S. Naval Research Lab Washington, D. C., 20390 Attn: Dr. William Zisman	1
Department of the Navy Washington, D.C. 20013 Attn: Bureau of Naval Weapons A. D. Nehman C. C. Singletorry Bureau of Ships Harry King	 1 1 1
Department of the Navy Naval Air Systems Command AIR-330 Washington, D. C. 20360	1
U.S. Navy Marine Engineering Lab Friction & Wear Division Annapolis Academy Annapolis, MD 21490 Attn: R. B. Snapp	1
Commanding Officer Eustis Directorate U.S. Army Air Mobility R&D Lab Ft. Eustis, VA 23604 Attn: John W. White, SAVDL-TD	1
U.S. Army Ordance Rock Island Arsenal Lab Rock Island, IL 61201 Attn: R. LeMar	1
AVCOM AMSAVEGTT Mart Building 405 S. 12th St. St. Louis, MO 63166 Attn: E. England	1

Addressee	Copies
Aerojet Liquid Rocket Company P.O. Box 13222 Sacramento, CA 95813 Attn: C. W. Williams	1
AiResearch Manufacturing Corp. 402 S. 36th St. Phoenix, AZ 85034 Attn: Dr. R. Blake Wallace	1
Avco Corp. Lycoming Division Stratford, CT 06497 Attn: R. Cuny	1
Battelle Memorial Institute Columbus Laboratories 505 King Ave. Columbus, OH 43201 Attn: C. M. Allen	1
Bendix Corp. Bendix Ctr. Southfield, MI 48075 Attn: M. J. Caparone	1
B. F. Goodrich Company Aerospace & Defense-Products Div. Troy, OH 45373 Attn: L. S. Blalkowski	1
Boeing Aircraft Co. 224 N. Wilkinson Dayton, OH 45402 Attn: H. W. Walker	1
The Boeing Company Vertol Division P.O. Box 16858 Philadelphia, PA 19142 Attn: A. J. Lemanski, MS P-32-09	1
Borg-Warner Corp. Ingersoll Research Ctr. Wolf and Algonquin Rds. Des Plaines, IL 60018	1

Addressee	Copies
Carborundum Co. Graphite Products Blank & Walmore Rds. Sanborn, NY 14132 Attn: R. M. Markel	1
Cartiseal Corp. 634 Glenn Ave. Wheeling, IL 60090	1
Chicago Rawhide Mfg. Co. 900 N. State St. Elgin, IL 60121	1
Gould, Inc. 17000 St. Clair Ave. Cleveland, OH 44110 Attn: J. Ross	1
Teledyne/CAE 1330 Laskey Rd. Toledo, OH 43601 Attn: R. J. Magrina	1
Crane Packing Co. 6400 W. Oakton St. Morton Grove, IL 60053 Attn: Harry Tankus	1
Defense Ceramics Information Ctr. Battelle Memorial Institute Columbus Labs. Room 11-9021 505 King Avenue Columbus, OH 43201	1
McDonnell-Douglas Corp. 333 West First St. Dayton, OH 45402 Attn: R. G. Donmoyer	1
Durametallic Corp. Kalamazoo, MI 49001 Attn: H. Hummer	1
Fairchild Industries, Inc. Republic Aviation Div. Farmingdale, LI, NY 11735 Attn: C. Collis	1

Addressee	Copies
Franklin Institute Research Labs 20th and Parkway Philadelphia, PA 19103 Attn: W. Shapiro	1
Garrett Corp. AiResearch Mfg. Div. 9851-9951 Sepulveda Blvd. Los Angeles, CA 90009 Attn: A. Silver	1
General Dynamics Corp. 1025 Connecticut Ave., SW Washington, D. C. 20036 Attn: George Villa	1
General Electric Company Advanced Engine & Technology Dept. Cincinnati, OH 45215 Attn: John Clark W. McCarty	1 1
General Motors Corp. Allison Division Plant #3, Dept. 7339 Indiannapolis, IN 46206 Attn: E. M. Deckman	1
Great Lakes Research Corp. 299 Park Ave. New York, NY 10017 Attn: J. P. Sachs	1
IIT Research Institute 10 West 35th St. Chicago, IL 60616 Attn: Dr. Strohmeier	1
Kendall Refining Co. Bradford, PA 16701 Attn: F. I.I. Lawrence	1
Koppers Co., Inc. Metal Products Division Piston Ring & Seal Dept. Baltimore, MD 21203 Attn: E. Taschenburg	1

Addressee	Copies
Lockheed Aircraft Co. 118 W. First St. Dayton, OH 45402 Attn: R. W. Witte	1
Los Alamos Scientific Lab. University of California Los Alamos, NM 87544 Attn: M. C. Smith	1
Martin Marietta Corp. P.O. Box 14153 Dayton, OH 45414 Attn: Z. G. Horvath	1
Mechanical Technology Inc. 968 Albany-Shaker Road Latham, NY 12110 Attn: D. F. Wilcock	1
Midwest Research Institute 425 Volker Blvd. Kansas City, MO 64110 Attn: V. Hopkins	1
Monsanto Chemical Co. 800 N. Lindberg Blvd. St. Louis, MO 63166 Attn: Dr. W. R. Richard R. Hatton	1 1
National Technical Information Service Springfield, VA 22151	40
North American Aviation Inc. 5100 W. 164 St. Cleveland, OH 44142 Attn: George Bremer	1
Northrop Corp. 1730 K Street, NW Suite 903-5 Washington, D.C. 20006 Attn: S. W. Fowler, Jr.	1

Addressee	Copies
Pesco Products Div. Borg-Warner Corp. 24700 N. Miles Bedford, OH 44146 Attn: W. J. Cieslik	1
Pressure Technology Corp. of America 453 Amboy Ave. Woodbridge, NJ 07095 Attn: A. Bobrowsky	1
Pure Carbon Co., Inc. 441 Hall Ave. St. Marys, PA 15857 Attn: J. J. Sherlock	1
Rocketdyne Division North American Rockwell Corp. 6633 Canoga Ave. Canoga Park, CA 91304 Attn: R. E. Burcham	1
Sealol Inc. P.O. Box 2158 Providence, RI 02905 Attn: Justus Stevens	1
Sikorsky Aircraft United Aircraft Corp. North Main St. Stratford, CT 06497 Attn: L. Burroughs	1
Sinclair Refining Co. 600 Fifth Ave. New York, NY 10020 Attn: C. W. McAllister	1
Sinclair Research Inc. 400 E. Sibley Blvd. Harvey, IL 60426 Attn: M. R. Farille	1

Addressee	Copies
SKF Industries, Inc. 1100 First Ave. King of Prussia, PA 19406 Attn: L. B. Sibley	1
Socony Mobil Oil Company Research Dept. Paulsboro Lab Paulsboro, NJ 08066 Attn: E. Oberright	1
St. Marys Co. 1939 State Road St. Marys, PA 15857 Attn: J. E. Lanzel	1
Director Government Research Lab Esso Research & Engineering Co. P.O. Box 8 Linden, NJ 07036	1
Southwest Research Institute P.O. Drawer 28510 San Antonio, TX 78284 Attn: P. M. Ku	1
Stanford Research Institute Menlo Park, CA 94025 Attn: R. C. Fey	1
Stein Seal Company 20th St. & Indiana Ave. Philadelphia, PA 19132 Attn: Dr. P. C. Stein	1
Sun Oil Company Automotive Laboratory Marcus, Hook, PA 19061 Attn: J. L. Griffith	1
United Aircraft Corp. Pratt & Whitney Aircraft East Hartford, CT 06108 Attn: R. Shevchenko, Engr. Bldg.	1

Addressee	Copies
Westinghouse Electric Corp. 5100 W. 164th St. Cleveland, OH 44142 Attn: Lynn Powers	1
Wright Aeronautical Division Curtiss-Wright Corp. 333 West First St. Dayton, OH 45402 Attn: D. Lombardo	1
The University of Tennessee Dept. of Mechanical & Aerospace Engr. Knoxville, TN 37916 Attn: Prof. W. K. Stair	1